scientific reports

Check for updates

OPEN

Groundwater contamination modelling in Ayad River Basin, Udaipur

Kuldeep Pareta

Groundwater, a vital freshwater resource catering to agricultural, domestic, and industrial needs, faces a pressing challenge of contamination due to escalating human activities. This study focuses on the Ayad River Basin in the Udaipur district of Rajasthan, employing the FEFLOW simulation code for the first time. A steady-state numerical model and a groundwater contaminant prediction model for total dissolved solids (TDS), nitrate, and fluoride were developed, simulating trends over the next five years with an accuracy exceeding 95%. The results reveal an eastward increase in TDS, nitrate, and fluoride concentrations, attributed to contamination from two waste disposal sites-Titadi and Baleecha. Titadi, operational for four decades until closure in 2010, retains residual waste over 32 thousand m². The initiation of a new dumping ground at Baleecha by the Udaipur Municipal Corporation post-2010 exacerbates regional contamination. Nitrate contamination is particularly high in agricultural zones with excessive chemical fertilizer usage. Of the 27 scenarios tested, 23 support using the water for irrigation but would require treatment before using it for drinking. Recommendations include deploying a chemical sensor network for real-time data input into the web enabled FEFLOW model, real-time monitoring and alerts, and a mobile application providing personalized guidance on water usage and health risks in case of contamination. This study can be beneficial to decision-makers, who work on the policy and groundwater management strategies.

Keywords Groundwater, Contamination, FEFLOW model, Ayad river, Udaipur

Water, essential for life, faces increasing risks due to significant changes in hydrology caused by climate change[1,2]. In this situation, groundwater plays a crucial role in maintaining regional water resource stability[3,4]. Ensuring reliable water supply requires a comprehensive approach that integrates surface and groundwater as a single hydrological resource[5,6]. Surface water and groundwater are closely linked and depend on each other[7–10]. Climatic and geographic factors create complex interactions between surface water and groundwater, so contamination in one often affects the other[11,12]. Human activities significantly contribute to groundwater pollution[13–18]. Practices like pesticide use in agriculture, industrial waste discharge, pipeline leaks, coal mining, and landfills significantly pollute groundwater, risking this essential resource[19–21]. Groundwater, like other water sources, is vulnerable to contamination, making rigorous monitoring and protection essential[22–25]. Groundwater and surface water interact in large landscapes due to many different factors[26,27]. Groundwater moves into and out of streams across the landscape, showing complex water flow patterns[28–30]. Understanding and managing how water systems are connected is crucial for using water resources sustainably[31–33].

Researchers use various methods to measure contaminants in groundwater. Groundwater modeling is a key approach to understand and predict how the system will behave in the future[34,35]. Groundwater models can be divided into physical, analogue, and mathematical types[36,37]. Physical models, like the Sand tank, show how groundwater works in a lab setting, but they can have scaling issues[38–40]. Analogue models use electronics to mimic water flow, while mathematical models use equations to represent groundwater systems, which can be solved with numbers or formulas[41–43]. Analytical models give exact answers for simple situations, while numerical models estimate solutions for more complex cases[44]. Prominent tools for measuring groundwater pollution include MODFLOW and FEFLOW, which provide good results[45–48]. Analytical models usually assume steady-state, one-dimensional conditions, but some, like analytical element models, can handle two-dimensional groundwater flow[49,50]. Contaminant transport models can use one-dimensional groundwater flow and one-, two-, or three-dimensional transport conditions[51–54]. Numerical models are widely used in practical applications for several reasons, primarily due to their versatility and ability to handle complex scenarios[55–57]. Numerical models are preferred in most practical applications due to their ability to manage complexity, flexibility, scalability,

nature portfolio

1

predictive capabilities, data integration, cost-effectiveness, and suitability for scenario testing. These advantages make them powerful tools for understanding and managing groundwater systems effectively. Modelers face a tough challenge in simplifying real-world problems accurately[58]. The accuracy of numerical models depends on precise data input, the size of steps used in space and time (larger steps can lead to more errors), and the method chosen to solve the model equations[59–62]. Paying attention to these details is crucial to make sure groundwater models are reliable for assessing and managing contamination effectively using scientific methods[63,64].

A detailed groundwater flow and contamination transport model has been carefully created for the Ayad River Basin, using the advanced features of the FEFLOW model. The primary objective is to conduct a comprehensive assessment of the probable concentrations of Total Dissolved Solids (TDS), nitrate, and fluoride within the affected area. Contaminant transport models play a crucial role by accurately simulating how contaminants move and change chemically underground alongside groundwater flow[36,65,66]. The model is advanced because it can accurately calculate how contamination levels of TDS, nitrate, and fluoride change month by month. Furthermore, it carefully shows how substances move and mix in the area where different water sources meet, giving detailed insights into how contaminants interact underground. The model results clearly show the vertical and horizontal spread of each contaminant. A notable contribution of this study is the pioneering generation of an empirical equation that correlates migration distance with time, presenting a quantifiable metric[67]. This innovative approach is a special addition to what we already know, making this study different from previous efforts in the field. The empirical equation offers a valuable tool for quantitative measurements, previously unexplored in the region. This novel methodology significantly advances our comprehension of contaminant dynamics in the Ayad River Basin, providing a robust foundation for informed decision-making in the realms of management and remediation strategies.

Rathore et al.[68] conducted a study on the Ayad River post its passage through Udaipur's urban and industrial areas. Sampling at points of domestic and industrial effluent discharge identified significant contamination, focusing on key parameters such as pH, temperature, conductivity, total dissolved solids (TDS), dissolved oxygen (DO), biochemical oxygen demand (BOD), chemical oxygen demand (COD), total organic carbon (TOC), acidity, alkalinity, total hardness, chloride, nitrate, phosphate, microbial population count (MPN), and heavy metals. Their findings highlighted severe pollution downstream of industrial discharge points. Kalal et al.[69] investigated surface water quality of the Ayad River, focusing on pollutants during June to August 2020. Parameters assessed included total hardness, TDS, chloride, sulphate, fluoride, iron, pH, BOD, COD, and DO. Elevated pollution levels were observed at industrial discharge points, with COD and BOD concentrations reaching 480.0 mg/l and 162.0 mg/l respectively, indicating severe organic pollution. Dhayachandhran et al.[70] conducted a GIS-based assessment of groundwater quality along the banks of the Adyar River. Their study identified issues such as high electrical conductivity, ion concentrations, and chloride dominance stemming from industrial and residential effluent discharge. Seawater intrusion exacerbated groundwater quality near coastal areas, necessitating robust management strategies for water quality improvement. In a groundwater quality study of the Banas River Basin, Pareta et al.[71] analyzed data spanning 2000–2018, emphasizing physico-chemical parameters. Significant contaminants identified included fluoride, nitrate, chloride, calcium carbonate ($CaCO_3$), and salts. Utilizing the Water Quality Index (WQI), the research revealed a declining groundwater quality index (GWQI) from west to east, with elevated salinity and hardness particularly noted in the eastern micro-watershed (MWS).

Groundwater flow and contaminant transport modeling present significant challenges, as noted by Diersch et al.[72], due to the complexity of managing spatially and temporally variable parameter fields. Integration of FEFLOW with GIS ARC/INFO addresses these challenges by providing a robust platform for managing parametric and geometric data, advanced computational tools, graphical visualization capabilities, and interactive data exchange functionalities. Sarma et al.[73] emphasize the increasing importance of simulating contaminant transport in both unsaturated and saturated groundwater zones, driven by rising water demands. Integrated models that consider interactions between these zones offer more accurate predictions compared to standalone models, crucial for effective regional groundwater management by better forecasting solute movements within groundwater systems. Kumar et al.[74] underscores the utility of groundwater contaminant transport models such as MODFLOW, MT3DMS, RT3D, FEFLOW, and MODPATH in predicting contamination behavior and facilitating management strategies. They stress the necessity for precise modeling objectives and appropriate tool selection to ensure accuracy and avoid errors in groundwater management practices.

This study focuses on assessing groundwater quality in the Ayad River Basin, located in Udaipur district, Rajasthan, using the FEFLOW simulation software. The primary objective is to develop a numerical model capable of predicting the spatial distribution and temporal trends of total dissolved solids (TDS), nitrate, and fluoride contamination over the next five years with a high accuracy exceeding 95%. The investigation addresses significant contamination challenges arising from human activities, particularly from historical and current waste disposal sites such as Titadi and Baleecha. The study aims to provide insights crucial for developing effective groundwater management strategies, emphasizing the importance of real-time monitoring and intervention to mitigate contamination impacts on agricultural and domestic water supplies in the region.

Study area

The Ayad River Basin, spanning 1207 km², is geographically positioned between 24°50′16″ to 24°27′46″ northern latitude and 73°31′44″ to 73°59′44″ eastern longitude. Administratively, it encompasses four tehsils (Girwa, Mavli, Vallabh Nagar, and Gogunda) in Udaipur district and one tehsil (Nathdwara) in Rajsamand district[75]. Originating from the Gogunda hills in north-west Udaipur, the Ayad River flows over a 68 km stretch before entering the Vallabh Nagar reservoir to the east of Udaipur (Fig. 1). As a seasonal river, it serves as a tributary to the Berach River, which, in turn, is a tributary to the Chambal River in the Yamuna basin. The Ayad River Basin experiences a tropical, semi-arid climate, characterized by summer temperatures ranging from 28.8 °C to 42.3 °C and winter
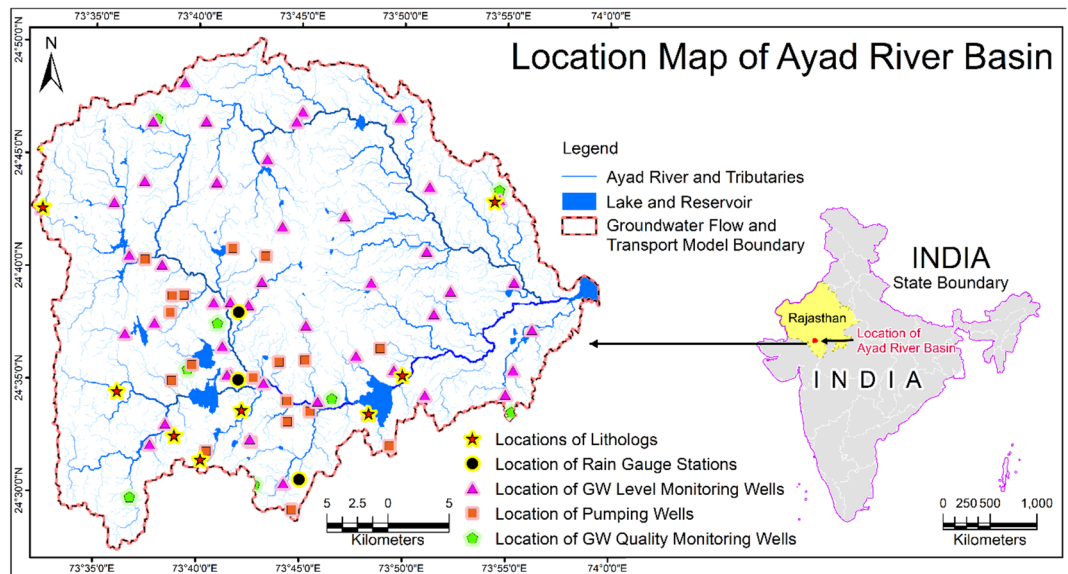
Figure 1. Location map of Ayad River Basin, Udaipur, and extents of the flow and transport model.

temperatures from 3.5 °C to 18.8 °C. The average annual rainfall is 640 mm, predominantly influenced by the southwest monsoon, delivering about 90% of the annual precipitation from July to mid-October. Groundwater, sourced from wells and hand pumps, constitutes 69% of the total irrigated area, with surface water contributing the remaining 31%.

Materials and methods
Data collection
This investigation leverages a comprehensive dataset, encompassing precipitation records from three raingauge stations, pumping rate data derived from 17 monitoring wells, hydraulic-head data collected from 45 groundwater monitoring wells, subsurface lithological information (lithologs) obtained from 11 borelogs, and groundwater quality data originating from 8 monitoring wells. These datasets were meticulously gathered from diverse sources, including the Water Resource Department (WRD), Govt. of Rajasthan; the College of Technology and Engineering (CTAE), Udaipur; the Ground Water Department (GWD), Govt. of Rajasthan; and the Central Ground Water Board (CGWB), Govt. of India.

Precipitation data
Precipitation data spanning from 2000 to 2022 was gathered from the Water Resource Department (WRD), Govt. of Rajasthan for three distinct rain gauge stations-namely, Udaipur (Girwa), Badgaon, and Biliya (Fig. 1). This comprehensive time series dataset was meticulously curated to serve as input for the FEFLOW model.

In 3D modeling, the flux boundary condition is characterized by the unit (L/T), denoting an influx of water across a defined area over a specific time. Given the presence of three distinct rain gauge stations, the basin boundary underwent segmentation into three delineated sections through the application of the Thiessen polygon method. Subsequently, all nodes within the top slice of the resultant Thiessen polygons were designated to represent rainfall-induced flow, thus establishing a comprehensive representation of the inflow dynamics across the basin boundary.

Monitoring wells data with pumping rate
The pumping rate data pertaining to the year 2016 was acquired from 17 monitoring wells locations, sourced from the College of Technology and Engineering (CTAE), Udaipur. The geographical distribution of these boreholes is visually represented in Fig. 1, with detailed information provided in the accompanying Table 1. These data points served as a foundational dataset for the estimation of critical hydraulic properties of the aquifer, including hydraulic conductivity and storage coefficient. This dataset was utilized to construct a robust model of the aquifer, enabling the estimation of its hydraulic properties. These hydraulic properties play a pivotal role in comprehending the dynamics of water flow within the aquifer, offering valuable insights for predicting future water availability and quality.

Hydraulic-head data
The hydraulic-head data encompassing both pre-and post-monsoon periods spanning from 2011 to 2022 were meticulously gathered from 45 groundwater monitoring wells, sourced from the Ground Water Department (GWD). Govt. of Rajasthan (Fig. 1). The application of a hydraulic-head boundary condition involves assigning a predetermined hydraulic head value to a specific node within the model. In contrast to calculating the hydraulic head as an outcome of the simulation, these nodes are characterized by having their head values predetermined

S. no	Pumping well name	X (m)	Y (m)	Total depth of the wells below land surface (m)	Z (top) m	Z (bottom) m	Well Type	Rate (flow) m³/d	Radius (m)	Type of aquifer	Wells, pumping from model layer
1	Baleecha, Goverdhan Vilas	365,749.17	2,713,589.79	05.03	613.24	608.21	MLW	276.0	2.66	Unconfined	Layer-1
2	Barhmnon Ka Guda	360,762.84	2,729,316.22	05.20	626.24	621.04	MLW	560.0	1.68	Unconfined	Layer-1
3	Bedwas	369,621.72	2,719,609.36	28.40	567.32	538.92	MLW	192.0	1.86	Unconfined	Layer-2
4	Bhilon Ka Bedla	370,660.78	2,729,564.44	05.60	806.62	801.02	MLW	639.0	2.94	Unconfined	Layer-1
5	Chikalwas	363,967.44	2,726,375.30	29.18	608.20	579.02	MLW	551.7	2.47	Unconfined	Layer-2
6	Dheenkli	373,863.14	2,721,035.09	28.20	585.05	556.85	MLW	579.0	4.61	Unconfined	Layer-2
7	Eklingpura	372,419.31	2,715,999.09	24.30	570.43	546.13	MLW	631.0	2.36	Unconfined	Layer-2
8	Eklingpura, Manwakhera	372,367.82	2,717,684.23	29.20	557.31	528.11	MLW	406.0	1.95	Unconfined	Layer-2
9	Farm Pond, CTAE	371,730.80	2,720,885.02	29.50	578.67	549.17	MLW	360.0	2.33	Unconfined	Layer-2
10	Gorela	362,928.29	2,719,386.51	21.97	617.60	595.63	MLW	588.0	2.50	Unconfined	Layer-2
11	Kaladwas	374,259.44	2,716,844.67	05.10	554.96	549.86	MLW	174.0	1.72	Unconfined	Layer-1
12	Kushal Bagh	369,431.44	2,714,329.75	29.00	594.78	565.78	MLW	503.0	2.57	Unconfined	Layer-2
13	Liyon Ka Guda	362,828.37	2,724,960.67	29.50	621.78	592.28	MLW	536.0	3.40	Unconfined	Layer-2
14	Manpura Lakhawali	367,958.65	2,730,192.22	22.04	625.06	603.02	MLW	654.0	2.36	Unconfined	Layer-2
15	Pheniyon Ka Guda	362,998.28	2,726,325.80	27.95	615.81	587.86	MLW	499.0	3.84	Unconfined	Layer-2
16	Rehta, Debari	380,024.96	2,721,982.43	24.20	551.59	527.39	MLW	516.0	3.11	Unconfined	Layer-2
17	Seesarma	364,608.30	2,720,673.43	04.25	608.45	604.20	MLW	475.0	3.65	Unconfined	Layer-1

Table 1. Pumping wells considered in the numerical model. *Source*: College of Technology and Engineering (CTAE), Udaipur[76].

by the boundary condition. This condition can result in either an inflow into the model when neighboring nodes exhibit lower potential or an outflow from the model in the presence of a gradient from neighboring nodes toward the boundary condition. Head boundary conditions find application in scenarios where the hydraulic potential is known in advance, such as in surface water bodies with a direct connection to groundwater, pump sumps maintaining a constant level for dewatering, or seepage faces in conjunction with a constraint condition.

Subsurface lithological information
Subsurface lithological information (lithologs) of 11 borelogs (Fig. 1) for year 2016 have been collected from Ground Water Department (GWD). Govt. of Rajasthan in hard copy format. The lithological log data has including of hydrological abstract, thickness, discharge, type of aquifer, yield test (V-NOTCH). By using this information, entire aquifer has been divided into 4 slices. These slices are slice-1 (0–6 m), slice-2 (6–30 m), slice-3 (30–70 m), and slice-4 (70–100 m) present the aquifer of the basin (Fig. 4). These 3D layer configuration has been used for switching the model type from 2 to 3D and vice versa, for setting up the basic 3D structure, or for changing the model layering later on. It has also used for creating layer pinch-outs using tetrahedral elements and for assigning elevations to the nodes.

Groundwater quality data
Groundwater quality data encompassing 16 key water quality parameters were gathered from the Ground Water Department (GWD), Govt. of Rajasthan, and the Central Ground Water Board (CGWB), Govt. of India for 8 locations, spanning the period between 2011 and 2022, as illustrated in Fig. 1. The GWD and CGWB diligently monitors groundwater quality during the months of May and June annually. The comprehensive set of water quality parameters includes pH (power of hydrogen, $-\log[H_3O^+]$), electrical conductivity (EC), total hardness in terms of calcium carbonate (TH, $CaCO_3$), total alkalinity (TA, $CaCO_3$), calcium (Ca^{2+}), magnesium (Mg^{2+}), sodium (Na^+), potassium (K^+), iron (Fe^{2+}), carbonate hardness (CO_3^{2-}), bicarbonate (HCO_3^-), chloride (Cl^-), sulfate (SO_4^{2-}), nitrate (NO_3^-), fluoride (F^-), and total dissolved solids (TDS). These parameters collectively contribute to a comprehensive analysis providing a general overview of groundwater contamination within the Ayad River Basin. Notably, among the 16 parameters, nitrate (NO_3^-), fluoride (F^-), and total dissolved solids (TDS) exhibit the most pronounced contamination levels in the study area. Consequently, these three critical groundwater quality parameters will serve as pivotal inputs for the forthcoming groundwater contamination modeling efforts within the Ayad River Basin.

Development of the numerical model

The finite difference method and finite element method stand out as predominant numerical approaches for solving groundwater flow or solute transport equations[77]. The selection between these methods hinges on the specific modeling objectives and the complexity of the issues under consideration. When dealing with intricate concerns, the finite difference method may yield divergent results compared to the finite element method[78]. It is crucial to note that the modeling approach alone does not singularly determine model outcomes; other factors, including initial conditions, boundary conditions, space discretization, and data quality, exert significant influence. In numerical modeling, hydrogeologists employ these methods to approximate solutions for intricate system differential equations by transforming them into discrete equations and partitioning the domain into grids or meshes. The dissection of a region and discretization of differential equations are typically accomplished using approximation techniques such as finite difference, finite element, and finite volume method. These methods can be employed individually or in combination to mitigate the computational complexity of numerical models. Each approach comes with its unique advantages and limitations, with considerations for applicability, ease of use, performance, and computational speed.

Modelling approach
The initial stage in any modeling endeavor involves delineating the model objectives. In the modeling process, meticulous attention is directed toward the acquisition and processing of data. Nonetheless, the pivotal step in modeling is the conceptualization of the model. Following the construction of the model and its preliminary execution, subsequent steps encompass calibration, verification, and sensitivity analysis. A graphical representation of the sequential stages in groundwater modeling is depicted in Fig. 2.

A numerical model for groundwater flow and contamination transport was constructed using the FEFLOW groundwater modeling software. FEFLOW was chosen for its distinctive advantages over alternative modeling systems, including the ability to employ flexible meshes essential for accommodating the 3D geometry of the model area. Additionally, FEFLOW's capability to conduct density-dependent flow modeling was crucial for capturing buoyancy effects associated with contamination layers.

The developed FEFLOW model was employed to analyze the dynamic behavior of nitrate, fluoride, and total dissolved solids contamination. Predictions were made regarding the expected duration of contamination over a specified period, 5 years. The outcomes of the model were instrumental in formulating strategies aimed at mitigating the average contamination levels of nitrate, fluoride, and total dissolved solids in abstracted water.

Formulating modelling objectives.   The main objective of this study is to investigate groundwater contamination in the Ayad River Basin. Specifically, the study aims to discern the current state of contamination and project future trends, focusing on key parameters such as nitrate (NO_3^-), fluoride (F^-), and total dissolved solids (TDS). The overarching goal is to employ the FEFLOW model to comprehensively analyze and quantify the extent of groundwater contamination. By doing so, it seeks to provide valuable insights into future trends, predicting whether the level of nitrate, fluoride, and TDS will rise of fall.

Model conceptualization.   Model conceptualization involves qualitatively describing a groundwater system by detailing the water balance, hydrological conditions, and aquifer characteristics[61]. It is a crucial stage in groundwater modeling, following the identification of model objectives, and requires data on aquifer properties, hydrology, boundary conditions, and hydraulic parameters[79-82]. A robust conceptual model should simplify real-world complexities while aligning with modeling goals and management needs, particularly in understanding contaminant transport and water flow dynamics.

For this study, the conceptual model included key factors such as flow and transport processes, model extent, spatial discretization, 3D mesh setup, structural geology, initial conditions, boundary conditions, recharge, material parameters, calibration, validation, water balance, and groundwater quality prediction. Once the conceptual model was developed, a mathematical model was created to represent the assumptions and equations of the
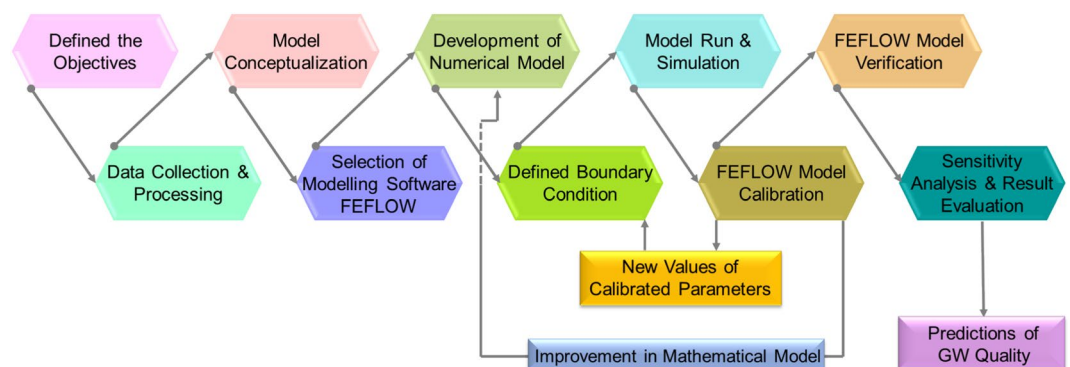
Figure 2. Modelling process flow chart.

conceptual model, which were solved through numerical methods. This approach ensured accurate predictions and effective management of groundwater quality in the Ayad River Basin.

Governing processes
Flow process.   The groundwater flow process is simulated, incorporating unsaturated flow effects through the utilization of the Richards' equation[83]. This equation, a simplified dual-phase model, efficiently captures water movement and desaturation effects, derived from the principles of mass and momentum conservation[84]. The Richards is expressed as:

$$\frac{\partial \theta}{\partial t} = \nabla \cdot \left[K(\theta) \left(\frac{\nabla \psi}{\gamma} - \mathbf{e}_z \right) \right]$$

where θ is the volumetric water content, t is time, $K(\theta)$ is the unsaturated hydraulic conductivity, ψ is the pressure head, γ is the unit weight of water, e_z is the unit vector in the vertical direction.

The equation describes how water content (θ) changes over time due to fluxes driven by gradients in pressure head (ψ) and the unsaturated hydraulic conductivity ($K(\theta)$). Richards' equation is crucial in modeling processes such as infiltration, groundwater recharge, and plant water uptake in agricultural and environmental studies. Its solutions provide insights into the movement and distribution of water in soils and other porous media under varying moisture conditions.

Transport process.   Contaminant migration is assessed through the advective–dispersive transport model within FEFLOW, integrating advective transport (associated with water movement) and dispersive/diffusive transport processes. During the steady-state calibration phase, no contamination transport is calculated. Nevertheless, a transport model for contaminants is introduced, incorporating a static (immobile) contaminant distribution to account for density effects during the steady-state calibration.

Density dependency.   Variations in contamination within the aquifers surrounding the Ayad river, and major lake, reservoir are recognized for their impact on the hydraulic system, primarily attributed to buoyancy forces. The model incorporates these buoyancy forces by employing a linear correlation between fluid density and disparities in nitrate, fluoride, and TDS concentrations.

Hydraulic and transport model extent
The hydraulic model shares the same spatial extent as the transport model, as depicted in Fig. 1. Utilizing this expanded model extent facilitates the utilization of natural features as boundary conditions, including (i) the surface catchment water divides to the west; (ii) the assumed boundary streamlines near the edge of the Ayad River Basin; and (iii) the Ayad River within the basin, along with major lakes and reservoirs in the central part of the basin. The total dimensions of the hydraulic flow model and transport model span 46.8 km in an east–west direction and 42.3 km in the north–south direction, covering an area of 1206.7 km². The vertical extent of the hydraulic model and transport model coincides with that of the ArcGIS 3D model, ranging from the highest point at 1011.45 m to the lowest point at 457.67 m.

Spatial discretization
The FEFLOW modelling software employs a flexible 3D meshing technology grounded in a 2.5D mesh geometry, wherein a completely unstructured 2D mesh is extruded over a designated number of layers with variable thickness, extending into a 3D domain. The layers can be made discontinuous by deactivating specific elements of the mesh, allowing for pinch-outs of geological layers. This process unfolds in two distinct steps, namely Horizontal 2D meshing and vertical 3D layer setup, elucidated in the subsequent sub-sections.

Horizontal discretization.   The primary aim of the horizontal mesh is to establish an optimal triangular mesh geometry that effectively approximates both human-made and natural features pertinent to the modelling process. Specifically, the relevant features for this modelling work include the flow model's domain extent, the transport model's domain extent, and the abstraction wells[85]. A secondary objective in this context is to ensure an average element size conducive to both the flow and transport models. The average element size in the outer basin and the inner area around the wells is approximately 1000 m and 10 m, respectively, with a smooth transition zone between them. Figure 3 illustrates the geometry of the finite element mesh. An effective measure of the 2D triangular mesh's quality is the distribution of triangle angles, ideally nearing 60° (equivalent to an equilateral triangle). A standard benchmark involves assessing the number of elements with angles larger than 90° or 120°. The present model exhibits excellent mesh quality, with only 0.1% of the mesh angles exceeding 90° and none surpassing 120°.

Layer configuration (3D mesh setup).   Density-dependent flow models, exemplified by the model discussed here, demand meticulous vertical discretization, particularly in regions with density gradients. FEFLOW, a finite-element model utilizing layered unstructured grids, provides significant flexibility to tailor model layers to diverse objectives[86]. Model layers, also known as numerical layers, may deviate from the geometric arrangement of hydrogeological layers (formations/units). In this context, three objectives guide the approach: maintaining model layer thickness within an acceptable range for accuracy and stability, ensuring element geometry
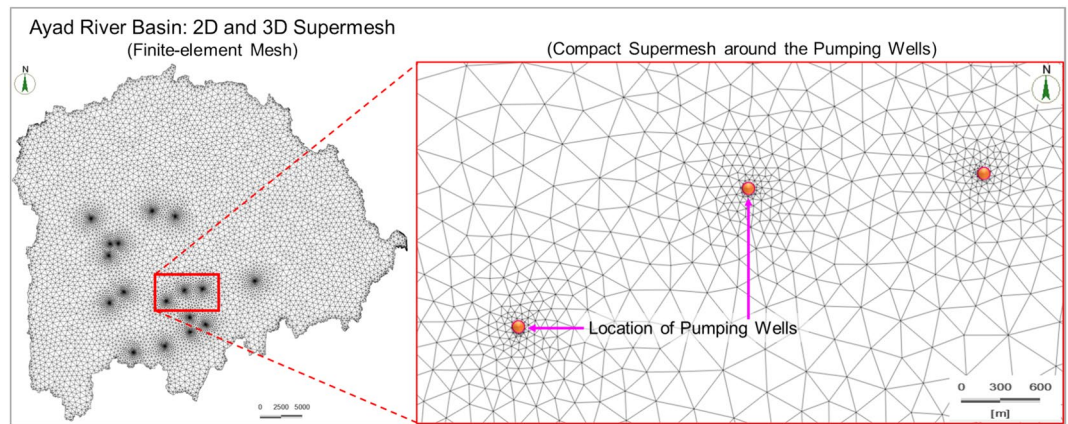
Figure 3. Finite-element mesh and compact supermesh in Ayad River Basin, Udaipur.
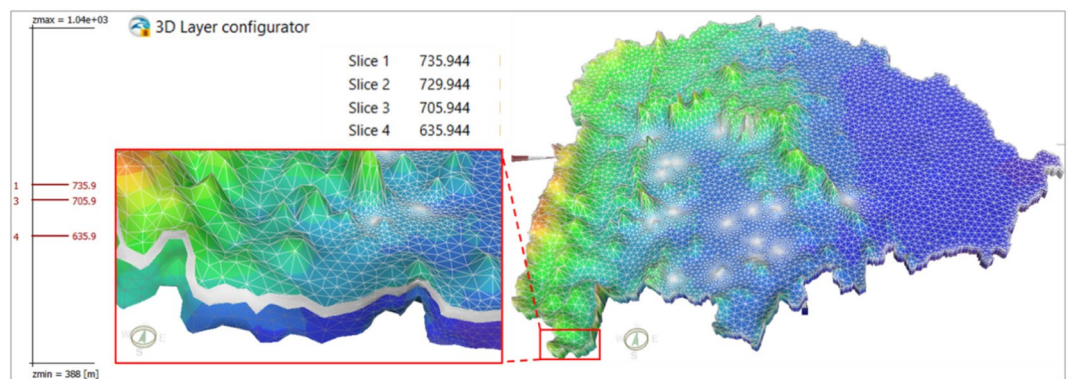

Figure 4. 3D finite-element mesh.

approximates geological contacts from the structural geological model, and minimizing the total number of elements for reasonable run-times.

These objectives are achieved through a combination of a stratigraphic layering approach, where geological and model layers consistently coincide, and a block model, wherein all layers are horizontal with a specified thickness. The extents of geological units are assigned based on their intersection with the model elements. The model incorporates a three-layer configuration to represent the subsurface geological conditions accurately. The first layer has an average thickness of 6 m, ranging from 735.94 m to 729.94 m above mean sea level (amsl). The second layer is 24 m thick, extending from 729.94 m to 705.94 m amsl. The third layer ranges from 705.94 m to 635.94 m amsl. The specific types of aquifers (confined or unconfined) within these layers have been detailed in Table 1. This layered structure is crucial for accurately simulating groundwater flow and contaminant transport dynamics across different depths. Figure 4 depicts the geometry of the resulting mesh, comprising 59.56 thousand active finite elements and containing 10.91 thousand active nodes.

Structural geology
The Ayad River Basin in Udaipur underwent an extensive geological examination, integrating diverse data sources, including the Geological Survey of India's 1:50,000 scale map, Landsat-9 OLI-2 + PAN satellite imagery (15 m resolution), and SRTM DEM data (30 m resolution)[75]. The resultant geological map, presented in Fig. 5, offers insights into rock types, lithology, and lineaments. The analysis reveals a spectrum of rock types spanning the Archaean to Upper Proterozoic eras, categorized into the Bhilwara, Aravalli, and Delhi supergroups[87]. Notably, the Archaean-era Mangalwar Complex, representing the Bhilwara supergroup, is situated approximately 55 km southwest of Chittorgarh[88]. The Gurali formation of the Debari group serves as a geological boundary, delineating the Bhilwara supergroup from the Aravalli supergroup[89]. The Aravalli Mountain range primarily comprises rocks from the Proterozoic-era Delhi Supergroup, with crystalline rocks from the Archaean age positioned between various geological formations, including the BGC/Bhilwara group, Aravalli supergroup, Palaeo-Proterozoic cover sequences, and Delhi fold belt rocks, equivalent to those in the BGC group[90]. This collaborative use of geological maps, satellite imagery, and elevation data has yielded a comprehensive understanding of the Ayad River Basin's geological composition, providing insights into its intricate and dynamic geological history.
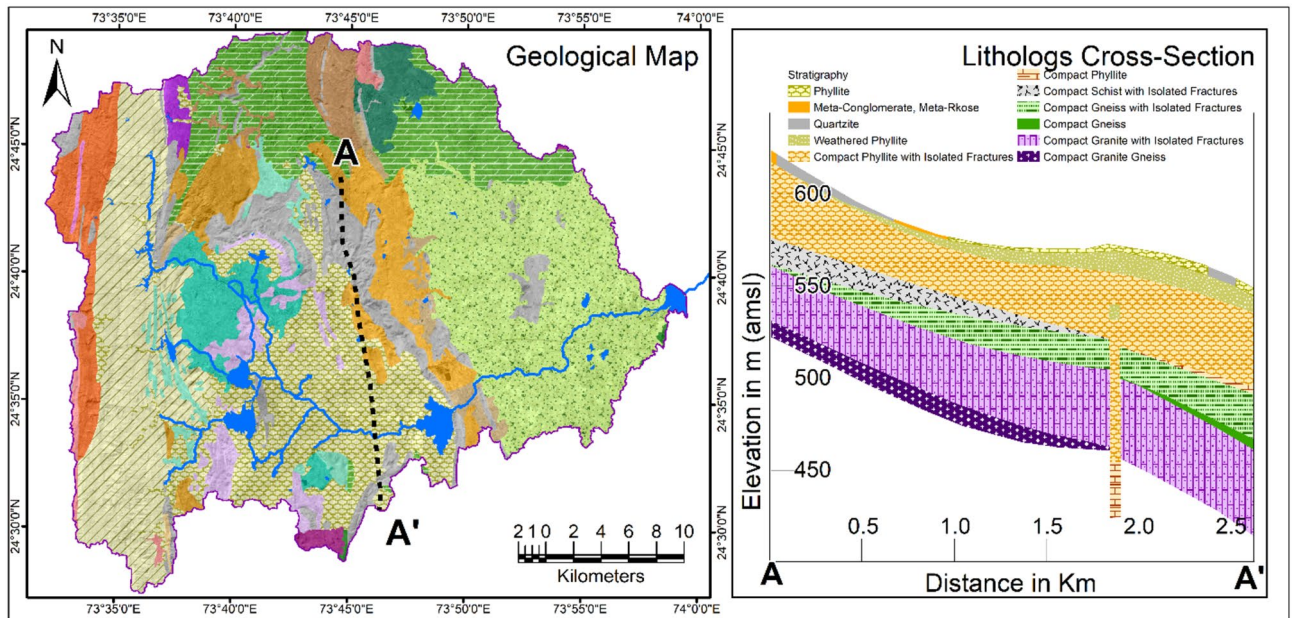
**Figure 5.** Geological map[91], and lithologs cross-section[92] of Ayad River Basin, Udaipur.

Following the successful generation of the 3D mesh, the model layers offer an effective approximation of the structural geological model. To facilitate the subsequent assignment of parameter values in FEFLOW, various sets or selections of finite elements are established in the FEFLOW model. These selections within FEFLOW are formulated by utilizing elevation data from each aquifer layer (slice), specifying the upper and lower extents of the slice, and incorporating 3D triangulated data for intrusion-type model objects.

Initial conditions
Hydraulic head/water levels.   The initial hydraulic head conditions for the transient modeling forecast are derived from a steady-state model run utilizing the parameter set specific to each scenario (Fig. 6).

Nitrate, fluoride, and TDS contamination.   The water quality parameters are examined to assess their conformity with the standards outlined by the World Health Organization (WHO), as delineated in Table 2. This rigorous evaluation is conducted to ascertain that the groundwater quality parameters align with the prescribed guidelines, ensuring their compliance with recommended standards for safe drinking water.

The spatial distribution maps of nitrate, fluoride, and Total Dissolved Solids (TDS) contamination in the Ayad River Basin were generated using the Inverse Distance Weighting (IDW) interpolation method in ArcGIS. IDW interpolation estimates values at unsampled locations based on the weighted average of nearby sampled values, where closer samples have higher influence. For this study, the average values of each contamination parameter from 2011 to 2022 were utilized. This method was chosen for its ability to effectively represent gradual changes
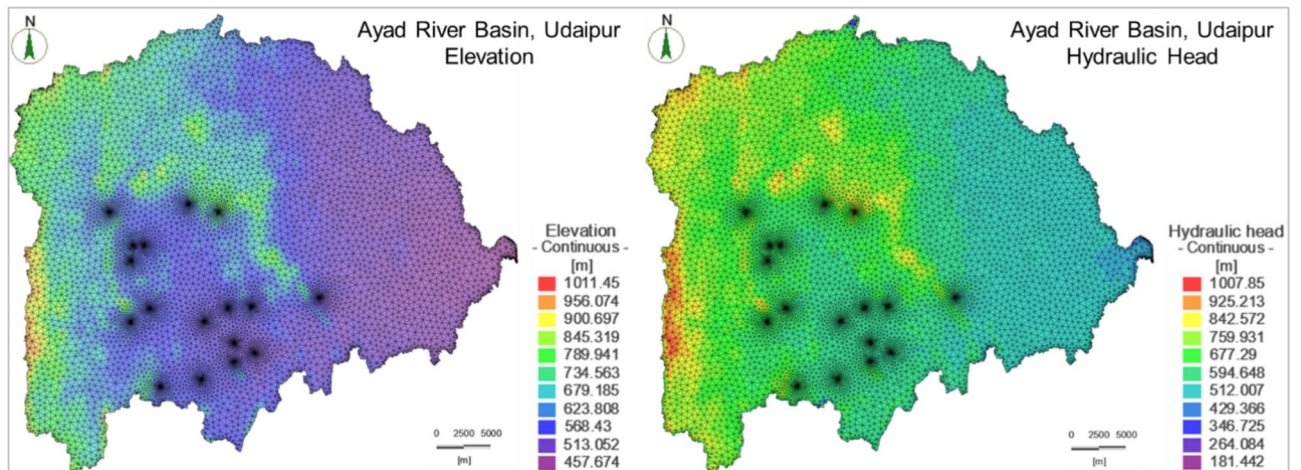
Figure 6. Elevation and hydraulic head in Ayad River Basin, Udaipur.

S. no	Water quality parameters	WHO[93]		Average data (2011–2022)		
		Desirable limit	Permissible limit	Min	Max	Ave
1	Nitrate (NO$_3^-$) mg/L	–	50	0.01	650.03	57.14
2	Fluoride (F$^-$) mg/L	0.6	4	0.01	4.13	0.58
3	Total dissolved solids (TDS) mg/L	500	1000	331.50	4270.50	1082.06

Table 2. Standards according to WHO protocols and observed ranges and averages.

in contamination levels across the basin, ensuring a continuous and spatially representative visualization of groundwater quality parameters. The spatial distribution of nitrate, fluoride, and TDS contamination in Ayad River Basin is sown in Fig. 7.

The lower thresholds for nitrate, fluoride, and total dissolved solids (TDS) contamination have been established in accordance with the permissible limits defined by the World Health Organization (WHO). This meticulous adherence to WHO standards ensures that the specified levels for these contaminants align with globally recognized guidelines, emphasizing a comprehensive approach to groundwater quality assessment.

Boundary conditions and recharge
<u>Pumping wells.</u> A total of 17 wells have been included in the model. Relevant well properties are listed in Table 1 and their locations are shown in Fig. 1. For each well, an additional one-dimensional finite element known as Discrete Feature Element (DFE) has been incorporated into the finite-element mesh. This element aligns with the actual dimensions of the well screen, defined by its top and bottom elevations, and emulates the conduit formed by the well screen. This inclusion facilitates water abstraction from all formations intersecting with the screen. The transmissivity of this element has been selected to match the anticipated screen diameter under the assumption of laminar flow, with intra-screen flow calculated using the Hagen-Poiseuille flow law.

Furthermore, each well is associated with a minimum water level, below which abstraction is not feasible. This minimum water level represents the depth at which the pump is positioned, and water abstraction is hindered if the water level falls below this threshold. Insufficient water abstraction may occur due to two main reasons: (i) the aquifers cannot yield an adequate amount of water, leading to a reduction in pumping rate to align with the aquifer yield; (ii) if the water level descends below the minimum hydraulic head, the well becomes deactivated, typically due to nearby pit dewatering activities.

<u>Recharge.</u> The model incorporates two distinct recharge systems: (i) diffusive (aerial) recharge applied at the surface. This recharge is implemented as an aerial source at the upper boundary of the model, representing net recharge. Rainfall data, obtained from three rain gauge stations in the Ayad River Basin, is utilized for this purpose, with model inputs derived through the thiessen polygons method based on these stations; (ii) recharge along drainage lines is depicted as a line source. Utilizing Shuttle Radar Topography Mission (SRTM) DEM data with 30 m spatial resolution (source: NASA Earth science data) and employing ArcGIS software, drainage lines are generated. All drainage lines are assumed to possess a uniform infiltration rate per unit length. The total net
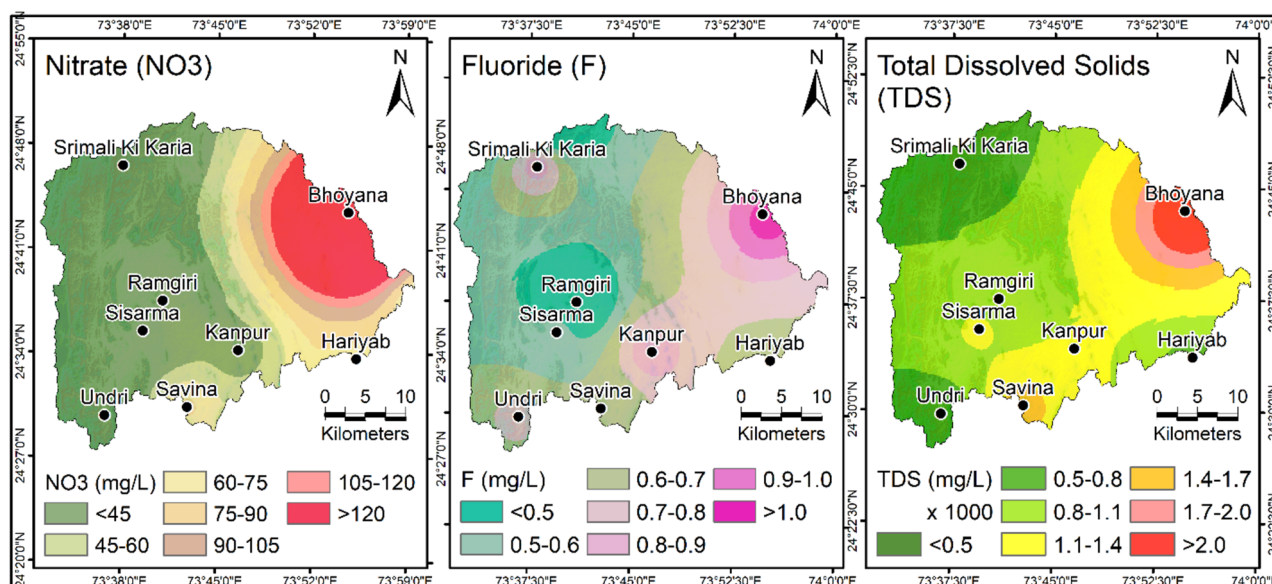
Figure 7. Spatial distribution of nitrate, fluoride, and TDS contamination in Ayad River Basin, Udaipur.

recharge is determined by the superposition of both effects. Each effect can be selected independently and has undergone calibration.

Material parameters
Material parameters are allocated as constant values to the main formations outlined by the structural geological model. This structure has been incorporated into the numerical model during the establishment of the hydrogeological structure. No additional zonation within the principal formation was introduced. This section elucidates the assumptions and data sources utilized to derive the parameter values.

Hydraulic conductivity.   FEFLOW facilitates the implementation of hydraulic conductivities in three distinct axes to accommodate anisotropy. In the present model, the orientation of these primary axes aligns with the main coordinate axes (K_{xx}, K_{yy}, and K_{zz}). The calibration process determines all hydraulic conductivity values (Table 3; Fig. 8). The hydraulic conductivity in horizontal directions (K_{xx} and K_{yy}) is presumed to be isotropic (K_{xx} and K_{yy} are identical) to streamline the degrees of freedom.

Specific yield and porosity.   The principal parameters influencing porosity in the FEFLOW model include the absolute porosity utilized in the flow model, referred to as "unsaturated porosity," and the porosity relevant to mass transport, termed "mass-transport porosity." Within the context of the unsaturated flow model, FEFLOW establishes saturation limits, defining both a residual saturation (lower limit) and a maximum saturation (upper limit). These parameters collectively implicitly define specific yield. To streamline complexity, default values for residual and maximum saturation (0.25% and 100%, respectively) are adopted, resulting in the negligible difference between absolute porosity and specific yield. The mass-transport porosity is assumed to be equal to specific yield, with a lower limit imposed to ensure model stability. Parameter values are selected based on relevant literature, with adherence to the LOM model principles whenever applicable. A detailed listing of these values is provided in Table 4.

Unsaturated parametric model.   The selection of the unsaturated model type necessitates the specification of parameters governing the water retention curve and the relative reduction of hydraulic conductivity concerning reduced saturation, encapsulated in the relative permeability relationship. At a regional scale, the significance of these parameters is generally mitigated, provided that the chosen values facilitate the infiltration of applied recharge. Consequently, a simplified van Genuchten model[95] has been employed for its pragmatic applicability. This model entails three distinct fitting parameters: alpha is determined on an element-wise basis as the reciprocal of the layer thickness. The van Genuchten parameters are set to default values in FEFLOW, namely $n = 1.964$ and $m = 0.4908$. This selection aims to ensure numerical stability while closely approximating actual capillary behavior. The relative permeability is configured to scale linearly with saturation, with the fitting parameter delta set to unity. This approach has demonstrated efficacy in optimizing both model stability and computational run times at the spatial scale under consideration. Typical parameters for a van Genuchten model are given in Table 5.

Calibration
The model parameters pertinent to flow, namely hydraulic conductivity, and recharge, encompassing the assumed head values at the reservoir and lakes, underwent calibration against mean water levels derived from a steady-state model. The primary goal of the calibration process was to ascertain a parameter set that concurrently meets the following criteria: (i) achieves a satisfactory fit between the model-derived water levels and observed

Component	Parameters	Unit	Prior range	Initial value	Range of model evaluations	Calibrated value
Geological layer-1 (sand/clay/silt/gravel) 0–6 m	K_{xx}	m/s	1×10^{-9}–1×10^{-2}	1×10^{-4}	2.4×10^{-6}–5.1×10^{-3}	4.2×10^{-5}
	K_{yy}	m/s	1×10^{-9}–1×10^{-2}	1×10^{-7}	1.0×10^{-5}–9.9×10^{-3}	6.1×10^{-4}
	S_y	–	0.00–0.35	0.15	0.01–0.33	0.26
	S_s	1/m	1×10^{-9}–1×10^{-2}	9.94×10^{-5}	5.6×10^{-5}–7×10^{-4}	8.6×10^{-5}
Geological layer-2 (weather and fractured: dolomitic limestone-sand-stone/granite-phyllite) 6–30 m	K_{xx}	m/s	1×10^{-9}–1×10^{-2}	1×10^{-4}	9.9×10^{-5}–1.5×10^{-8}	9.3×10^{-6}
	K_{yy}	m/s	1×10^{-9}–1×10^{-2}	1×10^{-7}	1.7×10^{-8}–9.9×10^{-6}	4.9×10^{-7}
	S_y	–	0.00–0.35	0.1	0.0–0.32	0.16
	S_s	1/m	1×10^{-9}–1×10^{-2}	6.89×10^{-4}	7.0×10^{-5}–5.3×10^{-4}	2.2×10^{-4}
Geological layer-3 (compact: phyllite, granite, schist, gneiss) 30–100 m	K_{xx}	m/s	1×10^{-9}–1×10^{-2}	1×10^{-4}	1.2×10^{-8}–3.3×10^{-3}	6.1×10^{-6}
	K_{yy}	m/s	1×10^{-9}–1×10^{-2}	1×10^{-7}	1.1×10^{-8}–9.4×10^{-4}	3.6×10^{-7}
	S_y	–	0.00–0.35	0.02	0.01–0.31	0.04
	S_s	1/m	1×10^{-9}–1×10^{-2}	3.68×10^{-6}	5.9×10^{-7}–4.9×10^{-6}	4.1×10^{-6}
Where:		K_{xx} = Horizontal hydraulic conductivity in X, K_{yy} = Horizontal hydraulic conductivity in Y, S_y = Specific yield, S_s = Specific storage				

Table 3. Hydraulic conductivity and specific yield.
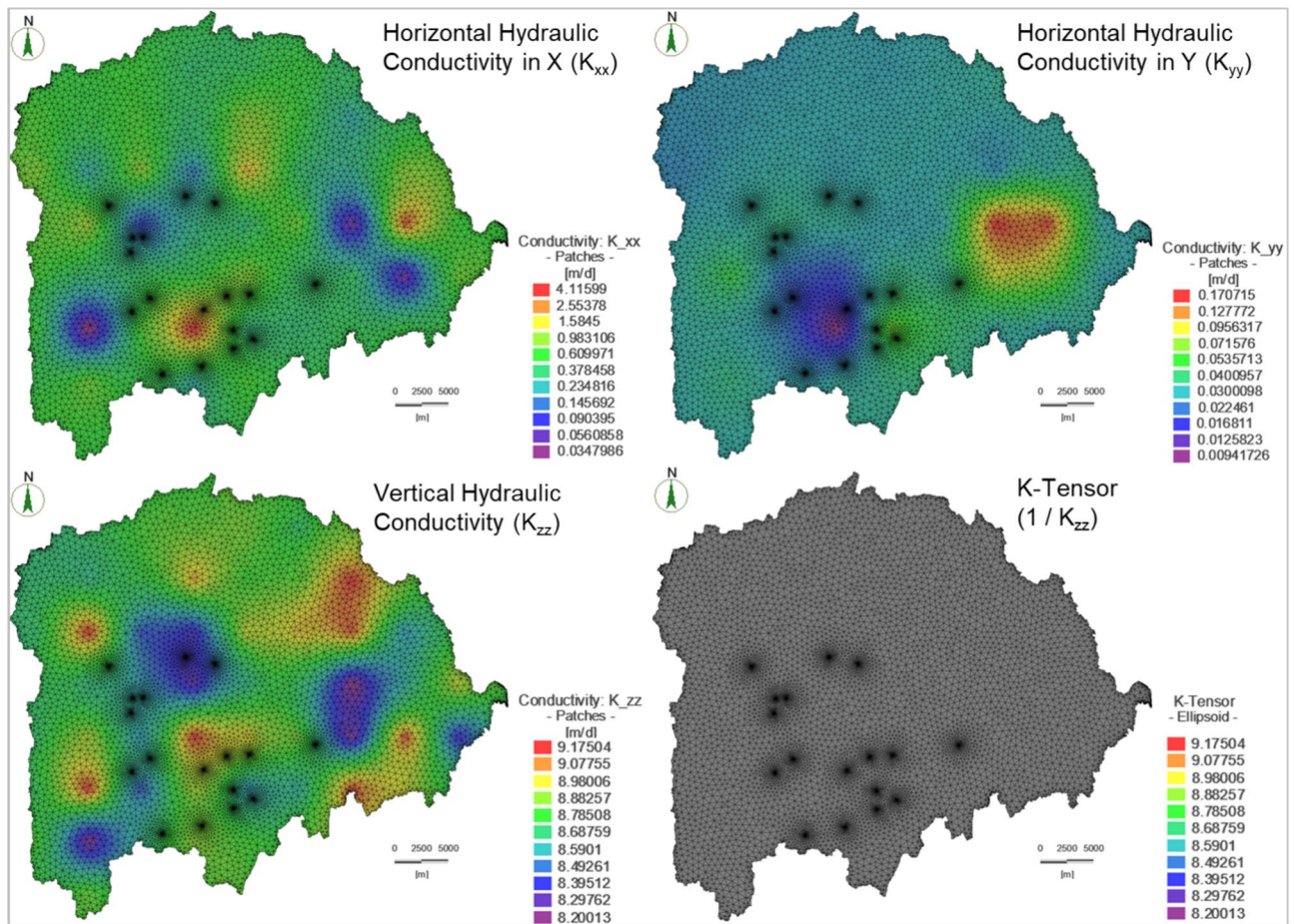
Figure 8. Hydraulic conductivity in the Ayad River Basin, Udaipur.

S. no	Unit	Porosity, pt	S. no	Unit	Porosity, pt
	Unconsolidated deposits			Rocks	
1	Gravel	0.25–0.40	1	Fractured basalt	0.05–0.50
2	Sand	0.25–0.50	2	Limestone	0.05–0.50
3	Silt	0.35–0.50	3	Sandstone	0.05–0.30
4	Clay	0.40–0.70	4	Dolomite	0.00–0.20
			5	Shale	0.00–0.10
			6	Fractured crystalline rock	0.00–0.10
			7	Dense crystalline rock	0.00–0.05

Table 4. Porosity values (applied in base case scenarios). *Source*: Freeze et al.,[94].

regional long-term water levels; (ii) maintains consistency with the prevailing understanding of local and regional hydrogeological conditions.

<u>Steady-state model setup.</u>   The model underwent an initial steady-state run, initially excluding the abstraction effects from pumps. For the subsequent transport model, an essential prerequisite was a reasonable approximation of the initial conditions for nitrate, fluoride, and total dissolved solids (TDS) contaminations, which were incorporated into the model at the commencement of the run. A static concentration distribution for nitrate, fluoride, and TDS was employed, with a caveat that the mass transport model could not be entirely deactivated, as calibration necessitated consistency with the hydraulic head in the transient forecasting model. It was observed that variations in nitrate, fluoride, and TDS distributions yielded significant differences in steady-state water levels. Calibration procedures were executed employing a dual approach, combining automated inverse modeling facilitated by an algorithm for parameter estimation within the PEST uncertainty estimation software, alongside manual adjustments.

S. no	Textural class	N	θ_r (cm³/cm³)	θ_s (cm³/cm³)	$\acute{\alpha}$ (1/cm)	n
1	Sand	126	0.058	0.37	0.035	3.19
2	Loamy sand	51	0.074	0.39	0.035	2.39
3	Sandy loam	78	0.067	0.37	0.021	1.61
4	Loam	61	0.083	0.46	0.025	1.31
5	Silt	2	0.123	0.48	0.006	1.53
6	Silt loam	101	0.061	0.43	0.012	1.39
7	Sandy clay loam	37	0.086	0.40	0.033	1.49
8	Clay loam	23	0.129	0.47	0.030	1.37
9	Silty clay loam	20	0.098	0.55	0.027	1.41
10	Silty clay	12	0.163	0.47	0.023	1.39
11	Clay	25	0.102	0.51	0.021	1.20

Table 5. Typical van Genuchten model parameters ($\acute{\alpha}$, n) including residual (θ_r), and saturated (θ_s) water contents compiles from the UNSODA database[96]. n indicates the number of soils or samples of a given textural class from which the mean values are compiled.

Calibration parameters.   **Hydraulic conductivity**
The calibration of hydraulic conductivity involves distinct adjustments for horizontal components (K_{xx} and K_{yy}) and the vertical component (K_{zz}), as detailed in Table 3. Zonation for hydraulic conductivity is delineated based on the primary geological units stipulated in the conceptual model (Section "Structural geology", structural geology).

Recharge.   Diffuse recharge: Recharge is administered as a function of specified fractions relative to the assumed mean annual precipitation rates, which are 819 mm/year for Udaipur (Girwa), 575 mm/year for Badgaon, and 1032 mm/year for Biliya. Distinct recharge factors are applied, delineating variations in the surface geological characteristics for the respective regions.
Drainage lines: Additional recharge is introduced along the drainage lines prevalent in the model area.

Consent to participate
By participating in this research on "Groundwater Contamination Modeling in Ayad River Basin, Udaipur" I consent to the utilization of my data for academic purposes.

Results and discussion
Calibration of hydraulic head
The calibration has been conducted using a combination of automated calibration through inverse modelling and manual calibration (using the parameter estimation capability of the PEST[97,98] calibration and uncertainty modelling software). Utilizing the Parameter ESTimation (PEST) tool embedded in the FEFLOW module, hydraulic head (groundwater level) simulations were conducted, as illustrated in Fig. 9. The fidelity of the simulation results reached an accuracy level of approximately 98%.
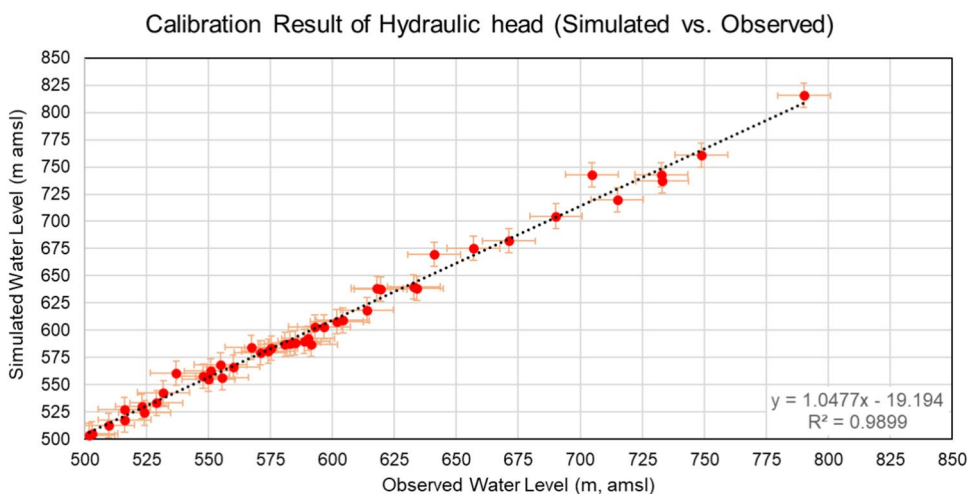
Figure 9. Calibration results of hydraulic head (simulated vs. observed).

Calibration of contaminant transport model

Calibration is the process of refining the model representation of the hydraulic properties to achieve a desired degree of correspondence between the model simulations and observations of the solute concentrations. In this study, calibration of contaminant transport model is achieved by adjusting the dispersivity values until the observed solute concentration matches with the calculated solute concentration. The TDS, nitrate, and fluoride concentrations in each groundwater monitoring well (observation well) are collected from SGWD, and CGWB. The calibration is stopped when a reasonable match between the observed and calculated concentration is achieved. After the calibration of contaminant transport model, the R^2 for TDS, nitrate, and fluoride contaminant transport model are obtained as 0.991, 0.994, and 0.958, respectively, and shown in Fig. 10. Longitudinal and transverse dispersivity values were modified by trial and error in order to match the observed and simulated values. Calibration shows that mass transport model is sensitive to dispersivity values. Table 6 gives the calibrated parameters of the contaminant transport model, and these are within the range reported by Gelhar et al.[99].

The overall mean error (ME), mean absolute error (MAE), root mean square error (RMSE), and R-squared value for groundwater level, and TDS, nitrate, and fluoride contamination are given in Table 7.

Groundwater quality prediction

Contaminant transport modeling has been conducted for three primary constituents: Total Dissolved Solids (TDS), nitrate (NO_3^-), and fluoride (F^-), which exhibit elevated concentrations in the Ayad River Basin. Concurrently, other parameters such as pH (measured as the negative logarithm of hydronium ion concentration, $-\log[H_3O^+]$), electrical conductivity (EC), total hardness as calcium carbonate (TH, $CaCO_3$), total alkalinity as calcium carbonate (TA, $CaCO_3$), calcium (Ca^{2+}), magnesium (Mg^{2+}), sodium (Na^+), potassium (K^+), iron (Fe^{2+}), carbonate hardness (CO_3^-), bicarbonate (HCO_3^-), chloride (Cl^-), and sulfate (SO_4^{2-}) exhibit relatively normal distribution. The presence of high TDS, nitrate, and fluoride concentrations in groundwater within the Ayad River Basin raises concerns due to their potential long-term adverse effects on human health if not adequately addressed. The developed model is employed to predict the travel distance of each of these three contaminants over a 5-year period. Alarming zones are identified in areas where contaminant concentrations
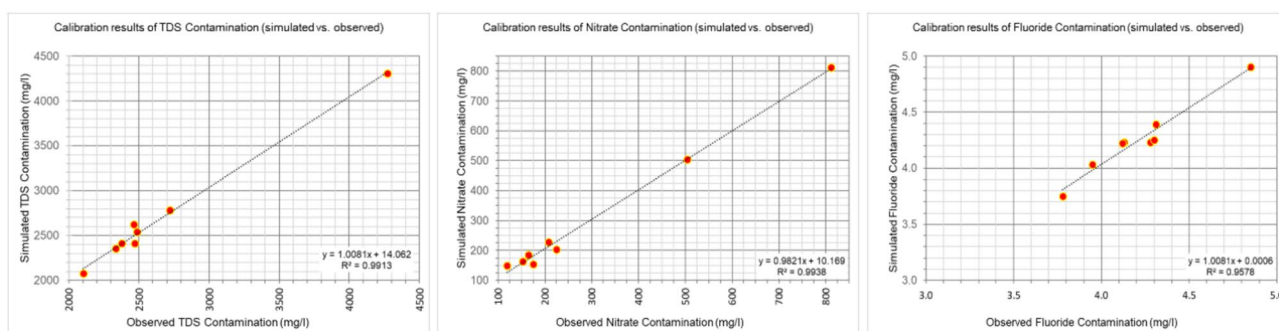

Figure 10. Calibration results of contaminant transport model (simulated vs. observed).

Aquifer material	Contamination type	Calibrated parameters reported by Gelhar et al.[99]			Calibrated parameters of this study			
		Hydraulic conductivity (m/s)	Effective porosity	Dispersivity	Dispersion (m)	Horizontal dispersivity	Vertical dispersivity	Diffusion coefficient (m²/d)
Unconfined aquifer	TDS	6.97×10^{-5}	0.33	30.5/9.11[100]	0.53	29.31	10.12	0.057
	Nitrate	9.55×10^{-5}	0.42	01.6/0.76[101]	0.52	01.42	00.74	0.048
	Fluoride	5.10×10^{-5}	0.26	10.0/2.02[102]	0.49	09.95	01.06	0.049

Table 6. Calibrated parameters of contaminant transport model.

Items	Total number of wells	Overall mean error (ME)	Mean absolute error (MAE)	Root mean square error (RMSE)	R-squared value
Groundwater monitoring wells (m)	45	9.32	9.53	12.40	0.989
TDS contamination (mg/l)	8	0.83%	1.30%	1.62%	0.991
Nitrate contamination (mg/l)	8	0.60%	1.89%	2.28%	0.993
Fluoride contamination (mg/l)	8	0.71%	1.38%	1.46&	0.957

Table 7. Overall mean error (ME), mean absolute error (MAE), root mean square error (RMSE), and R-squared value for groundwater level, and TDS, nitrate, and fluoride contamination.

surpass established standard limits. The permissible limits are defined in accordance with the guidelines set forth by the WHO[93].

The execution of the prediction model was carried out without accounting for water abstraction through pumping activities. This baseline run serves the purpose of validating the quasi-steady state assumption concerning the initial distribution of Total Dissolved Solids (TDS), nitrate, and fluoride. The rationale behind this validation lies in assessing whether the TDS, nitrate, and fluoride distribution, established under quasi-steady state conditions, would remain relatively unchanged over an extended simulation period in the absence of pumping-induced disturbances. The baseline run provides insights into the displacement of TDS, nitrate, and fluoride resulting from natural water movement, allowing an evaluation of the assumption that the background water movement is insignificantly small compared to the TDS, nitrate, and fluoride movement induced by water production activities. This assumption neglects the effect of background movement, considering it to be negligible in comparison to the impact of TDS, nitrate, and fluoride movement attributed to water extraction. To ascertain the validity of this assumption, the prediction model was executed under natural, undistorted conditions, enabling the observation and analysis of the background movement of TDS, nitrate, and fluoride within the system.

Total dissolved solids (TDS)
The contaminant transport model specifically targeting total dissolved solids (TDS) underwent a phased development, initially being executed for multiple time periods. Subsequently, a decision was made to limit the model's simulation to a duration of 5 years. The refined model was then executed for the designated 5-year period. Post-simulation, the cross-sectional data for each groundwater monitoring well (observation well) was meticulously extracted, which is presented in Fig. 11. This process ensures a focused examination of the temporal and spatial distribution of TDS within the groundwater system, providing valuable insights into the contaminant's behavior and impact over the specified time frame.

Upon comprehensive analysis of well locations within the Ayad River Basin, notable variations in the 500 mg/l total dissolved solids (TDS) feature emerge. Specifically, at Bhoyana and Kanpur, the feature extends up to 320 m from the observation well. This substantial extension could be attributed to diverse sub-surface lithological characteristics, hydraulic conductivity variations, and porosity dynamics. In contrast, other locations such as Srimali ki Karia, Undri, Sisama, Ramgiri, and Savina exhibit a comparatively shorter reach of the 500 mg/l TDS feature, extending up to 200 m from the observation well. Notably, at Hariyab, the same feature reaches only 140 m from the observation well.

Considering the permissible limit set at 1000 mg/l, it is observed that TDS levels increase significantly in the eastward direction at all locations. The distinct patterns in TDS distribution underscore the influence of local hydrogeological factors and emphasize the need for targeted interventions to curb the rapid increase in TDS levels, particularly in the eastern region of the study area. This detailed assessment provides valuable insights for implementing strategic measures to mitigate and manage TDS contamination effectively.

Nitrate
The nitrate contaminant transport model has been executed, mirroring the approach applied to the total dissolved solids (TDS) contaminant transport model, spanning a 5-year period. Analysis of the forecasted data reveals compelling patterns when considering the permissible limit of 50 mg/l for nitrate. Noteworthy observations include the 50 mg/l features extending approximately 340 m from the observation well in Srimali Ka Karia, Ramgiri, Savina, and Hariyab. In Bhoyana, the same feature reaches 240 m from the observation well, while in Undri, Sisarma, and Kanpur, the feature extends up to 500 m (Fig. 12). Although no explicit correlation with subsurface lithology is evident in the features pattern in all observation wells, a discernible influence of weathered/fractured rocks, characterized by varying hydraulic conductivity and porosity, is noted. The nitrate contaminants in all groundwater monitoring wells (observation wells) exhibit an eastward movement, aligning with the direction of groundwater flow.

Upon analyzing the land use, temperature, and rainfall dynamics within the Ayad River Basin, a discernible positive correlation emerges between the percentage of cropland in a specific area and the concentration of nitrate in groundwater. Notably, environmental factors, including temperature and precipitation, play pivotal roles as co-factors in this relationship. Higher average temperatures exhibit an inversely proportional relationship with nitrate contamination in groundwater, a phenomenon potentially attributed to increased evapotranspiration processes. Concurrently, increased average precipitation serves to dilute nitrates within the soil, consequently leading to a reduction in groundwater nitrate concentration. These findings underscore the multifaceted interplay between land use, climatic elements, and groundwater quality, offering valuable insights into the complex dynamics of nitrate contamination in the study area. The primary driver of nitrate contamination in the region is identified as the excessive use of chemical fertilizers. A crucial recommendation emerges to curtail this source of contamination, advocating for the adoption of natural (organic) fertilizers as a more sustainable alternative. This strategic shift aligns with the broader objective of mitigating nitrate contamination in the study area.

Fluoride
The fluoride contaminant transport model underwent a simulation analogous to the TDS and nitrate contaminant transport models, spanning a 5-year period. Despite the permissible limit for fluoride contaminants in all groundwater monitoring wells (observation wells) being within the acceptable range of 4 mg/l[93], there has been limited spatial movement observed. Over the 5-year modeling period, fluoride contaminant (4 mg/l) has extended up to 20 m from the observation wells, with a discernible eastward trend mirroring the groundwater flow (Fig. 13). The presence of fluoride in groundwater stems from the weathering and leaching of fluoride-bearing minerals within rocks and sediments.
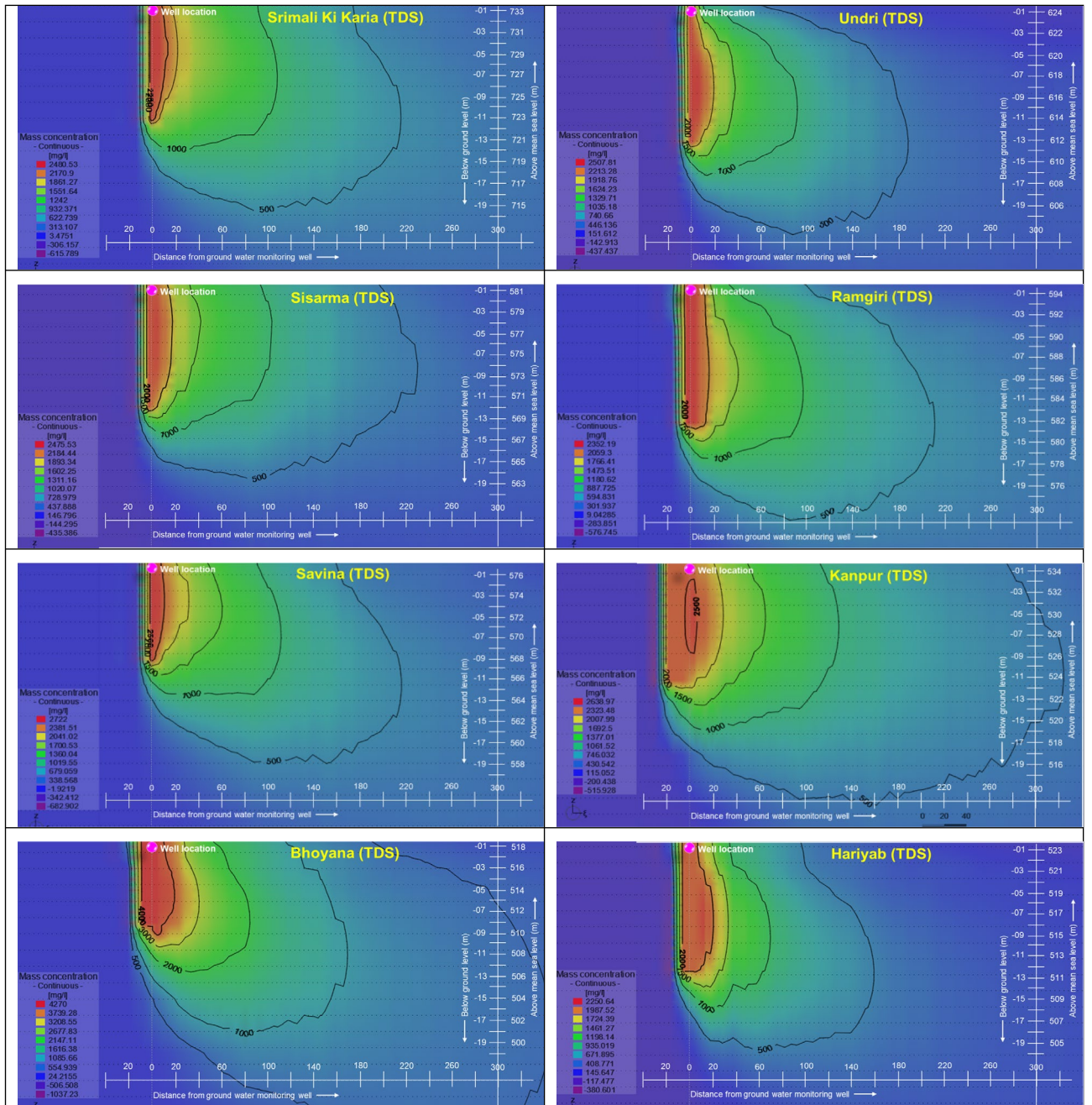
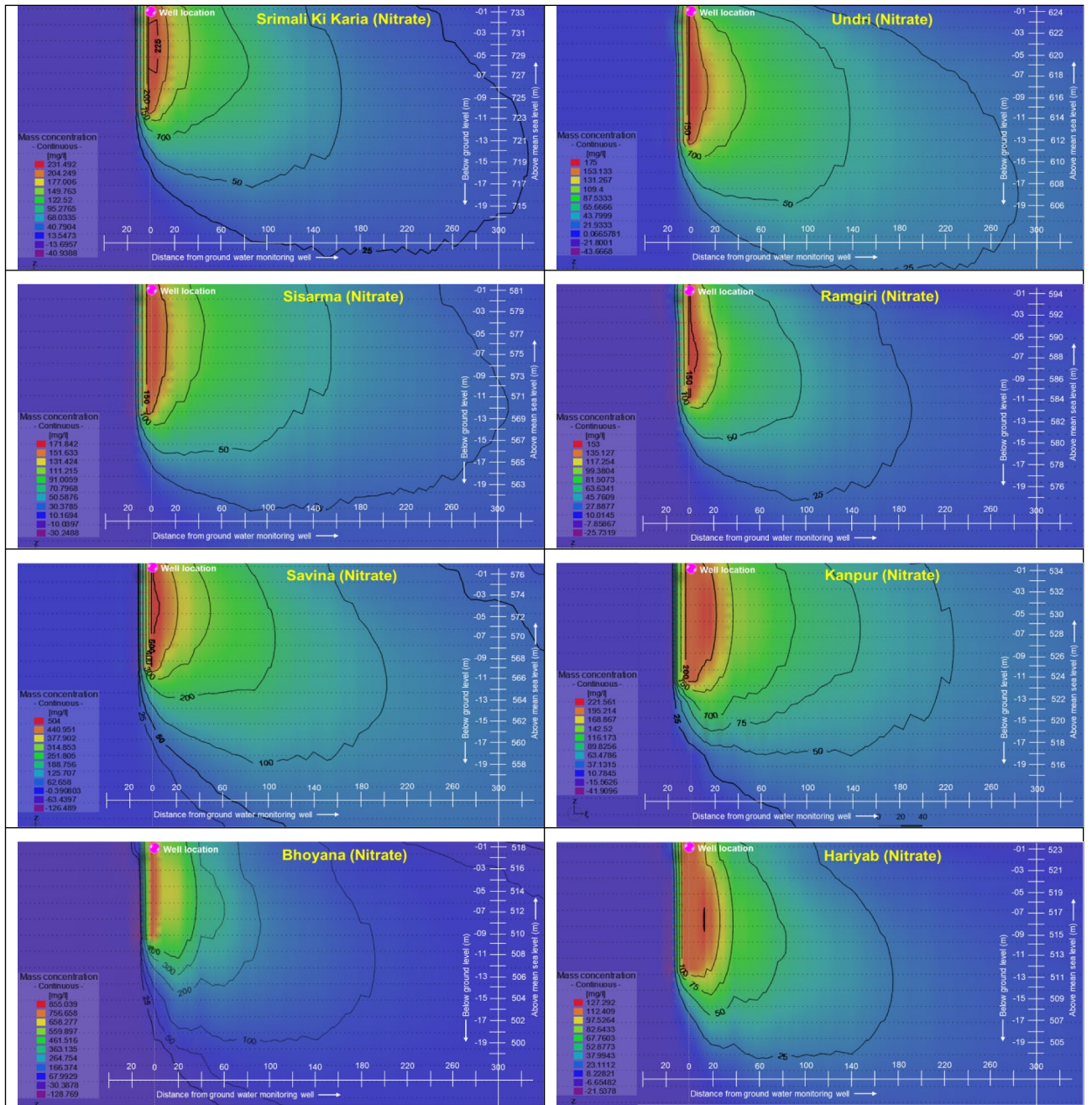**Figure 11.** Contaminant transport model result for TDS (travel distance 5 years).

Ingesting fluoride in modest amounts (< 0.5 mg/L) offers dental health benefits by reducing dental caries. However, higher concentrations (> 4 mg/L) may lead to fluorosis. While fluoride levels are currently low in Ayad River Basin, practical strategies should be developed to ensure the provision of fluoride-safe drinking water to rural communities in the region. This emphasizes the need for ongoing monitoring and mitigation efforts to safeguard public health in the face of potential fluctuations in fluoride concentrations.

Sensitivity analysis

Conducting a global sensitivity analysis necessitates the exploration of parameters at various levels, typically involving three distinct levels within the parameter space. Various strategies exist to achieve this objective, ranging from the manipulation of individual parameter values, as seen in the one-at-a-time (OAT) test plan, to the execution of extensive sets of random parameter values through Monte-Carlo Simulations. These methodologies differ in terms of numerical complexity, the labour-intensive nature of model establishment, and their effectiveness in discerning the sensitivity of parameters and their combinations[103].

The study employs the fractional factorial test design (FFD) method[104]. In this experimental design, all parameters are tested at three levels: base case, lower level, and upper level. This ensures that any primary effects
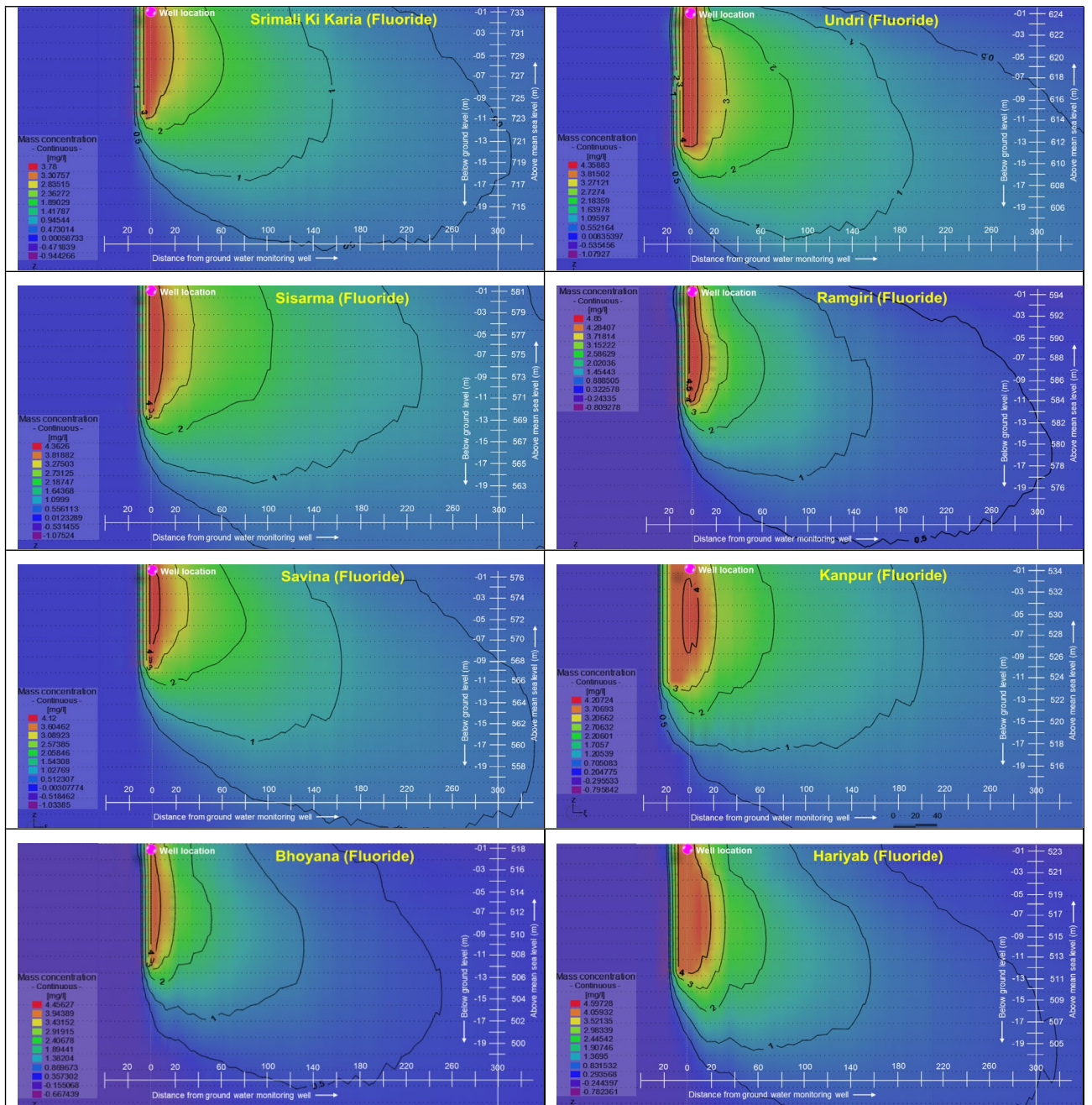
Figure 12. Contaminant transport model result for nitrate (travel distance 5 years).

of individual parameters remain unconfounded by combination effects of order two. A total of 27 scenarios are necessary to execute the test plan fully. For each of the 27 parameter sets outlined in the test plan, both a steady-state model (configured identically to the calibration model) and a contaminant transport model (configured similarly to the water quality assessment model) are generated.

Initially, the steady-state model is executed, providing a hydraulic head distribution for assessing the model-to-measurement misfit compared to the calibrated base case. Scenarios with unacceptably large residuals, indicating inconsistency with observed field data, are excluded from the sensitivity study. For scenarios demonstrating satisfactory calibration quality, the predictive run is conducted, utilizing the results of their respective steady-state models as initial hydraulic head conditions. As the test plan favors extreme parameter values, some sets may potentially strain the model beyond stability limits. Therefore, model scenarios undergo testing for numerical performance, and transient runs exhibiting unstable behavior are eliminated from the study.

A series of steady-state scenarios were formulated and executed, with resulting water level distributions exported and compared to the primary calibration target. Each model's calibration quality was classified based on the model-to-measurement misfit: (i) very good (residual generally less than 0.5 m), (ii) good (most residual around 1 m or below), (iii) okay (most residual around 2 m or below), (iv) acceptable (most residual around 3 m

Figure 13. Contaminant transport model result for fluoride (travel distance 5 years).

or below), (iv) moderate (most residual around 5 m or below), and (v) unacceptable (most residual exceeding 5 m). Table 8 details the classification for each model run, guiding the rejection or acceptance decision.

Conclusion

A numerical model based on the groundwater modelling software FEFLOW has been developed with the purpose of estimating the expected water quality in the Ayad River Basin, and prediction the affected area over the next 5 years. This model meticulously evaluates the concentrations of total dissolved solutes (TDS), nitrate, and fluoride, crucial for irrigation and domestic water supply in the Ayad River Basin. The established threshold concentrations stand at 2000 mg/l for TDS, 50 mg/l for nitrate, and 4 mg/l for fluoride. Calibration of the model involved a comprehensive approach, relying on average steady-state water levels and incorporating prior knowledge of expected parameter values derived from aquifer test evaluations. Additionally, a thorough sensitivity analysis was executed to estimate the anticipated variations in model results due to inherent uncertainties associated with parameter values. This analytical process aimed to pinpoint the influential parameters contributing to the observed variations, enhancing the model's reliability and predictive capabilities.

| Scenario | Model-to-measurement fit | | | Scenario | Model-to-measurement fit | | |
	Wells in Ayad River Basin	Raw water supply	Decision		Wells in Ayad River Basin	Raw water supply	Decision
1	Okay (+)	Acceptable (+)	Accepted	15	Okay (+)	Moderate (+)	Accepted
2	Okay (+)	Acceptable (+)	Accepted	16	Moderate (+)	Inacceptable (+)	**Rejected**
3	Good (−)	Good (+)	Accepted	17	Moderate (+)	Inacceptable (+)	**Rejected**
4	Acceptable (+)	Okay (+)	Accepted	18	Very good (0)	Good (+)	Accepted
5	Inacceptable (+)	Inacceptable (+)	**Rejected**	19	Moderate (−)	Moderate (−)	Accepted
6	Good (+)	Okay (+)	Accepted	20	Okay (−)	Acceptable (−)	Accepted
7	Moderate (−)	Acceptable (−)	Accepted	21	Good (−)	Good (+)	Accepted
8	Okay (−)	Okay (+)	Accepted	22	Okay (−)	Okay (−)	Accepted
9	Good (−)	Okay (+)	Accepted	23	Moderate (−)	Moderate (−)	Accepted
10	Good (−)	Good (0)	Accepted	24	Moderate (−)	Moderate (−)	Accepted
11	Good (+)	Inacceptable (+)	**Rejected**	25	Moderate ( )	Moderate (−)	Accepted
12	Acceptable (−)	Good (−)	Accepted	26	Good (−)	Good (−)	Accepted
13	Good (−)	Okay (+)	Accepted	27	Acceptable (−)	Acceptable (−)	Accepted
14	Good (−)	Okay (+)	Accepted	Scenario source: ESH[104]			

Table 8. Model-to-measurement fit of sensitivity scenarios. Significant values are in bold.

The calibrated steady-state model and contaminant transport model exhibit an impressive accuracy exceeding 95%. According to the contaminant prediction model, TDS levels demonstrate a substantial increase in the eastward direction across all locations. These discernible patterns in TDS distribution underscore the localized hydrogeological influences, emphasizing the necessity for targeted interventions to mitigate the rapid escalation of TDS levels, particularly in the eastern region of the study area. High levels of total dissolved solids (TDS), nitrate, and fluoride contamination are prominently observed in the eastern and southeastern region of the Ayad River Basin. This phenomenon can be attributed to the presence of two waste disposal sites, namely Titadi and Baleecha. Titadi, a landfill in operation for four decades until its closure in 2010, still exhibits residual waste covering an area of 32,000 m². Concurrently, the initiation of a new dumping ground at Baleecha by the Udaipur Municipal Corporation (UMC) post-2010 has contributed to the exacerbation of contamination in the specified regions. Upon scrutinizing land use, temperature, and rainfall dynamics within the Ayad River Basin, a notable positive correlation emerges between the percentage of cropland in a specific area and the concentration of nitrate in groundwater. The primary driver of nitrate contamination is attributed to the excessive use of chemical fertilizers. A critical recommendation advocates curbing this contamination source by transitioning to natural (organic) fertilizers as a more sustainable alternative. While fluoride levels are currently low in the Ayad River Basin, practical strategies need development to ensure the provision of fluoride-safe drinking water to rural communities in the region. This underscores the imperative for ongoing monitoring and mitigation efforts to safeguard public health in anticipation of potential fluctuations in fluoride concentrations (Table 8).

The sensitivity analysis, conducted through the fractional factorial test design (FFD) method, encompassed a total of 27 model-to-measurement fit scenarios. Out of these, 23 scenarios received acceptance, signifying that water can be used for irrigation purposes. However, treatment is deemed necessary before considering the supply for drinking purposes. This comprehensive analysis and decision-making framework contribute to informed water management strategies.

Scope of future work

Some idea for groundwater quality analysis that has not been widely explored is the use of artificial intelligence (AI) techniques in combination with groundwater quality modelling using FEFLOW model.

- Sensor network deployment: should be set up a network of chemical sensors specifically designed to detect various contaminants in groundwater, such as heavy metals, nitrates, TDS, fluoride, pesticides, or organic pollutants. These sensors should be connected to FEFLOW model through MIKE OPERATIONS Web that can collect and transmit real-time data to web. FEFLOW model should be run automatic every day at a particular time and should be display the predictive modeling result on the MIKE OPERATIONS Web.
- Real-time monitoring and alerts: should be implemented a real-time monitoring system that continuously analyzes the incoming data from the sensor network, and model prediction result. If the system detects any sudden changes or anomalies in groundwater quality beyond specified thresholds, it should generate alerts to notify relevant stakeholders, such as water resource management authorities or local communities.
- Mobile application: should be developed a user-friendly mobile application that allows individuals, such as farmers or residents in affected areas, to access groundwater quality information in real-time. The application can provide personalized recommendations for water usage, awareness about potential health risks, and suggestions for alternative water sources if contamination is detected.

Data availability

The datasets used and analysed during the current study available from the corresponding author on reasonable request.

References

1. Stott, P. A. *et al.* Attribution of extreme weather and climate-related events. *WIREs Clim. Change* **7**(1), 23–41. https://doi.org/10.1002/wcc.380 (2016).
2. FAO. The impact of disasters and crises on agriculture and food security: 2021. *Rome* https://doi.org/10.4060/cb3673en (2021).
3. Zektser, I. S., & Everett, L. G. *Groundwater Resources of the World and Their Use*. IHP-VI, Series on Groundwater No. 6 (2004). https://unesdoc.unesco.org/ark:/48223/pf0000134433
4. Ternes, B. Groundwater citizenship and water supply awareness: Investigating water-related infrastructure and well ownership. *Rural Sociol.* https://doi.org/10.1111/ruso.12179 (2018).
5. UNDP. *A Holistic Approach to Addressing Water Resources Challenges in Yemen, UNDP Strategic Framework* (2022). United Nations Development Programme (UNDP), Republic of Yemen. https://www.undp.org/sites/g/files/zskgke326/files/2022-11/2022%20Nov%20Water%20Resources%20Challenges%20in%20Yemen.pdf
6. Dinsa, H. T. & Nurhusein, M. M. Integrated water resources management stumbling blocks: Prioritization for better implementation under Ethiopian context. *Heliyon* **9**(e18785), 1–18. https://doi.org/10.1016/j.heliyon.2023.e18785 (2023).
7. Richts, A., Struckmeier, W., & Zaepke, M. WHYMAP and the Groundwater resources of the world. In *Sustaining Groundwater Resources. International Year of Planet Earth* (eds Jones, J.S.) (Springer, 2011). https://doi.org/10.1007/978-90-481-3426-7_10
8. Foster, S. & Ait-Kadi, M. Integrated water resources management (IWRM): How does groundwater fit in?. *Hydrogeol. J.* **20**, 415–418. https://doi.org/10.1007/s10040-012-0831-9 (2012).
9. BGR & UNESCO. *River and Groundwater Basins of the World* (World-Wide Hydrogeological Mapping and Assessment Programme (WHYMAP), 2024). https://www.whymap.org/whymap/EN/Maps_Data/Rgwb/rgwb_node_en.html. Access on 2nd January 2024.
10. USGS. *Interaction of Ground Water and Surface Water in Different Landscapes* (United States Geological Survey (USGS), 2024). https://pubs.usgs.gov/circ/circ1139/pdf/part1bb.pdf. Access on 2nd January 2024.
11. Schiedek, D., Sundelin, B., Readman, J. W. & Macdonald, R. W. Interactions between climate change and contaminants. *Marine Pollut. Bull.* **54**(12), 1845–1856. https://doi.org/10.1016/j.marpolbul.2007.09.020 (2007).
12. Noyes, P. D. *et al.* The toxicology of climate change: Environmental contaminants in a warming world. *Environ. Int.* **35**(6), 971–986. https://doi.org/10.1016/j.envint.2009.02.006 (2009).
13. Cosgrove, W. J. & Loucks, D. P. Water management: Current and future challenges and research directions. *Water Resour. Res.* **51**, 4823–4839. https://doi.org/10.1002/2014WR016869 (2015).
14. Green, T. R. Linking climate change and groundwater. In *Integrated Groundwater Management* (eds. Jakeman, A. J., Barreteau, O., Hunt, R. J., Rinaudo, J. D., Ross, A.) (Springer, 2016). https://doi.org/10.1007/978-3-319-23576-9_5
15. Li, P., Karunanidhi, D., Subramani, T. & Srinivasamoorthy, K. Sources and consequences of groundwater contamination. *Arch. Environ. Contam. Toxicol.* **80**(1), 1–10. https://doi.org/10.1007/s00244-020-00805-z (2021).
16. Cheng, C. *et al.* What is the relationship between land use and surface water quality? A review and prospects from remote sensing perspective. *Environ. Sci. Pollut. Res.* **29**, 56887–56907. https://doi.org/10.1007/s11356-022-21348-x (2022).
17. Sarkar, S., Mukherjee, A., Senapati, B. & Duttagupta, S. Predicting potential climate change impacts on groundwater nitrate pollution and risk in an intensely cultivated area of South Asia. *ACS Environ.* **2**, 556–576. https://doi.org/10.1021/acsenvironau.2c00042 (2022).
18. Irfeey, A. M. M., Najim, M. M. M., Alotaibi, B. A. & Traore, A. Groundwater pollution impact on food security. *Sustainability* **15**, 4202. https://doi.org/10.3390/su15054202 (2023).
19. Abhilash, P. C. & Singh, N. Pesticide use and application: An Indian scenario. *J. Hazard. Mater.* **165**, 1–12. https://doi.org/10.1016/j.jhazmat.2008.10.061 (2009).
20. Antoine, M. K., & Marnik, V. *Explaining Nitrate Pollution Pressure on the Groundwater Resource in Kinshasa Using a Multivariate Statistical Modelling Approach* (EGU General Assembly, 2013). https://ui.adsabs.harvard.edu/abs/2013EGUGA..15.9509M/abstract
21. FAO. *Thematic Papers on Groundwater* (Food and Agriculture Organization of the United Nations (FAO), 2016).
22. Sasakova, N. *et al.* Pollution of surface and ground water by sources related to agricultural activities. *Front. Sustain. Food Syst.* https://doi.org/10.3389/fsufs.2018.00042 (2018).
23. Carrard, N., Foster, T. & Willetts, J. Groundwater as a source of drinking water in Southeast Asia, and the Pacific: A multi-country review of current reliance and resource concerns. *Water* **11**(8), 1605. https://doi.org/10.3390/w11081605 (2019).
24. Grönwall, J. & Danert, K. Regarding groundwater and drinking water access through a human rights lens: Self-supply as a norm. *Water* **12**(2), 419. https://doi.org/10.3390/w12020419 (2020).
25. Baig, F., Sherif, M., Sefelnasr, A. & Faiz, M. A. Groundwater vulnerability to contamination in the Gulf Cooperation Council region: A review. *Groundw. Sustain. Dev.* https://doi.org/10.1016/j.gsd.2023.101023 (2023).
26. Sophocleous, M. Interactions between groundwater and surface water: the state of the science. *Hydrogeol. J.* **10**(1), 52–67. https://doi.org/10.1007/s10040-001-0170-8 (2002).
27. USGS. *Natural Processes of Groundwater and Surface-Water Interaction* (United States Geological Survey (USGS), 2024). https://pubs.usgs.gov/circ/circ1139/htdocs/natural_processes_of_ground.htm. Access on 2nd January 2024.
28. Belcher, W. R., & Sweetkind, D. S. (Eds.). *Death Valley Regional Groundwater Flow System, Nevada, and California-Hydrogeologic Framework and Transient Groundwater Flow Model*. U.S. Geological Survey Professional Paper 1711, 398 p (2010). https://pubs.usgs.gov/pp/1711/
29. Doulatyari, B., Basso, S., Schirmer, M. & Botter, G. River flow regimes and vegetation dynamics along a river transect. *Adv. Water Resour.* **73**, 30–43. https://doi.org/10.1016/j.advwatres.2014.06.015 (2014).
30. Weatherl, R. K. *Groundwater Contamination, Recharge, and Flow Dynamics in the Anthropogenic Environment* (University of Neuchâtel, 2020). https://www.dora.lib4ri.ch/eawag/islandora/object/eawag:22131
31. Tzanakakis, V. A., Paranychianakis, N. V. & Angelakis, A. N. Water supply and water scarcity. *Water* **12**, 2347. https://doi.org/10.3390/w12092347 (2020).
32. Guo, Q. Strategies for a resilient, sustainable, and equitable Mississippi River basin. *River* **2**, 336–349. https://doi.org/10.1002/rvr2.60 (2023).
33. Li, P. & Wu, J. Water resources and sustainable development. *Water* **16**, 134. https://doi.org/10.3390/w16010134 (2024).
34. Li, J., Lu, W., Wang, H. & Fan, Y. Groundwater contamination source identification based on a hybrid particle swarm optimization-extreme learning machine. *J. Hydrol.* **584**(3), 124657. https://doi.org/10.1016/j.jhydrol.2020.124657 (2020).
35. Zaresefat, M. & Derakhshani, R. Revolutionizing groundwater management with hybrid AI models: A practical review. *Water* **15**, 1750. https://doi.org/10.3390/w15091750 (2023).

36. Bear, J., & Cheng, A. H. D. *Modeling Groundwater Flow and Contaminant Transport* (Springer, 2010). https://doi.org/10.1007/978-1-4020-6682-5

37. EPA. *Ground Water Modeling Research* (United States Environmental Protection Agency (EPA), 2024). https://www.epa.gov/land-research/ground-water-modeling-research (Access on 2nd January 2024)

38. Hakoun, V., Mazzilli, N., Pistre, S. & Jourde, H. Teaching groundwater flow processes: Connecting lecture to practical and field classes. *Hydrol. Earth Syst. Sci.* **17**, 1975–1984 (2013).

39. Anderson, M. P., Woessner, W. W., & Hunt, R. J. *Applied Groundwater Modeling, Simulation of Flow and Advective Transport*, 2nd edn (Elsevier, 2015). https://doi.org/10.1016/C2009-0-21563-7

40. Yusuf, H. *et al.* Physical modeling of sand columns application in recharge reservoir to prevent seawater intrusion. *Water Supply* **22**(2), 2170–2178. https://doi.org/10.2166/ws.2021.365 (2022).

41. Robinove, C. J. *Ground-Water Studies and Analog Models*. Geological Survey Circular 468 (U.S. Geological Survey, 1962). https://pubs.usgs.gov/circ/1962/0468/report.pdf

42. Elango, L. *Numerical Simulation of Groundwater Flow and Solute Transport* (Allied Publishers Pvt. Ltd., 2005). https://luk.staff.ugm.ac.id/aat/pdf/NumericalSimulationOfGroundwaterFlow.pdf

43. Barnett, B., Townley, L. R., Post, V., Evans, R. E., Hunt, R. J., Peeters, L., et al. *Australian Groundwater Modelling Guidelines* (Waterlines report, National Water Commission, 2012).

44. Hayek, M., Kosakowski, G. & Churakov, S. Exact analytical solutions for a diffusion problem coupled with a precipitation–dissolution reaction and feedback of porosity change. *Water Resour. Res.* https://doi.org/10.1029/2010WR010321 (2011).

45. Yamagata, K., Butts, M. B., Grooss, J., Clausen, T. H., Graham, D. N., Clausnitzer, V., Gründler, R., & Monninkhoff, B. *OpenMI Coupling of FEFLOW and MIKE SHE. 34th Hydrology and Water Resources Symposium* (2012). https://www.dhigroup.com/upload/publications/mikeshe/Yamagata_2012.pdf

46. Guzman, J. A. *et al.* A model integration framework for linking SWAT and MODFLOW. *Environ. Model. Softw.* **73**, 103–116. https://doi.org/10.1016/j.envsoft.2015.08.011 (2015).

47. Mensah, J. K. *et al.* Integrated modeling of hydrological processes and groundwater recharge based on land use land cover, and climate changes: A systematic review. *Environ. Adv.* https://doi.org/10.1016/j.envadv.2022.100224 (2022).

48. Chowdhury, A. & Rahnuma, M. Groundwater contaminant transport modeling using MODFLOW and MT3DMS: A case study in Rajshahi City. *Water Pract. Technol.* **18**(5), 1255–1272. https://doi.org/10.2166/wpt.2023.076 (2023).

49. Ackerman, D. J., Rousseau, J. P., Rattray, G. W., & Fisher, J. C. *Steady-State and Transient Models of Groundwater Flow and Advective Transport, Eastern Snake River Plain Aquifer, Idaho National Laboratory and Vicinity*, Idaho: U.S. Geological Survey Scientific Investigations Report 2010-5123 (2010). https://pubs.usgs.gov/sir/2010/5123_B/pdf/sir20105123.pdf

50. Zhang, Y. *Groundwater Flow and Solute Transport Modeling* (University of Wyoming, 2016). https://geofaculty.uwyo.edu/yzhang/files/gwmodelcoursenoteoutline.pdf

51. Singh, M. K., Rajput, S. & Singh, R. K. Study of 2D contaminant transport with depth varying input source in a groundwater reservoir. *Water Supply* **21**(4), 1464–1480. https://doi.org/10.2166/ws.2021.010 (2021).

52. Zeynali, M. J. *et al.* Development of a contaminant concentration transport model for sulfate-contaminated areas. *Appl. Water Sci.* **12**, 169. https://doi.org/10.1007/s13201-022-01689-1 (2022).

53. Shu, X., Wu, Y., Zhang, X. & Yu, F. Experiments and models for contaminant transport in unsaturated and saturated porous media—A review. *Chem. Eng. Res. Des.* **192**, 606–621. https://doi.org/10.1016/j.cherd.2023.02.022 (2023).

54. Deng, H. *et al.* Efficient calibration of groundwater contaminant transport models using Bayesian optimization. *Toxics* **11**(5), 438 (2023).

55. Harbaugh, A. W., et al. *MODFLOW-2000, the US Geological Survey Modular Ground-Water Model: User Guide to Modularization Concepts and the Ground-Water Flow Process* (US Geological Survey, 2000).

56. Zheng, C. & Bennett, G. D. *Applied Contaminant Transport Modeling* Vol. 2 (Wiley, 2002).

57. Meca, A. S., López, F. A. & Fernández, C. G. Density-driven flow and solute transport problems. A 2-D numerical model based on the network simulation method. *Comput. Phys. Commun.* **177**(9), 720–728. https://doi.org/10.1016/j.cpc.2007.06.008 (2007).

58. Schmid, F. Understanding and modeling polymers: The challenge of multiple scales. *ACS Polym. Au* **3**(1), 1–140. https://doi.org/10.1021/acspolymersau.2c00049ope (2023).

59. Lal, A. M. W. Numerical errors in groundwater and overland flow models. *Water Resour. Res.* **36**(5), 1237–1247. https://doi.org/10.1029/2000WR900018 (2000).

60. Trabucchi, M., Fernàndez-Garcia, D. & Carrera, J. Automatic calibration of groundwater models with Bias correction and data filtering: Working with drawdown data. *Water Resour. Res.* **57**, e2020WR028097. https://doi.org/10.1029/2020WR028097 (2021).

61. Menichini, M. *et al.* Groundwater modeling with process-based and data-driven approaches in the context of climate change. *Water* **14**(23), 3956. https://doi.org/10.3390/w14233956 (2022).

62. Nyende, J., Enyogoi, I., Mango, J. & Kasumba, H. Numerical simulation of a two-dimensional groundwater pollutes transport problem using incompressible steady-state Navier–Stokes equations and diffusion-convection equations. *Model. Simul. Eng.* **2022**, 7419502. https://doi.org/10.1155/2022/7419502 (2022).

63. Norouzi Khatiri, K. *et al.* Groundwater management and allocation models: A review. *Water* **15**(2), 253. https://doi.org/10.3390/w15020253 (2023).

64. Karuppannan, S. *et al.* Chemical contamination of groundwater: Sources, geochemical mechanisms, health risks, and remediation. *J. Chem.* **6**, 66 (2023).

65. Banerjee, A., Creedon, L., Jones, N., Gill, L. & Gharbia, S. Dynamic groundwater contamination vulnerability assessment techniques: A systematic review. *Hydrology* **10**(9), 182. https://doi.org/10.3390/hydrology10090182 (2023).

66. Seyedpour, S. M., Thom, A. & Ricken, T. Simulation of contaminant transport through the Vadose Zone: A continuum mechanical approach within the framework of the extended theory of porous media (eTPM). *Water* **15**(2), 343. https://doi.org/10.3390/w15020343 (2023).

67. FEFLOW *8.0 Documentation—Introduction* (2023). Retrieved 19 December 2023, from https://download.feflow.com/html/help80/feflow/01_Introduction/intro.htm

68. Rathore, D. S., Rai, N. & Ashiya, P. Physico chemical analysis of water of Ayad River at Udaipur, Rajasthan (India). *Int. J. Innov. Res. Sci. Eng. Technol.* **3**(4), 66 (2007).

69. Kalal, V., Giri, M. N., Baskar, S. & Kuba, R. Detection of pollutants present in the surface water of Ayad River, Udaipur, Rajasthan. *Int. J. Biol. Innov.* **3**(1), 212–220 (2021).

70. Dhayachandhran, K. S. & Jothilakshmi, M. Quality assessment of ground water along the banks of Adyar river using GIS. *Mater. Today Proc.* **45**(7), 6234–6241. https://doi.org/10.1016/j.matpr.2020.10.587 (2021).

71. Pareta, K. & Pareta, U. Hydro-geochemical analysis of groundwater of a micro-watershed (MWS) of Banas River Basin, Rajasthan, India. *Int. J. Environ. Chem.* **9**(1), 1–22 (2023).

72. Diersch, H. J., Kaden, S., Michels, I. 3D/2D modeling of groundwater flow and contaminant processes—The simulation system FEFLOW coupled with GIS ARC/INFO. In *Contaminated Soil'93. Soil & Environment* (eds. Arendt, F., Annokkée, G. J., Bosman, R., Van Den Brink, W. J.) vol. 2 (Springer, 1993). https://doi.org/10.1007/978-94-011-2018-0_73

73. Sarma, R. & Singh, S. K. Simulating contaminant transport in unsaturated and saturated groundwater zones. *Water* https://doi.org/10.1002/wer.1555 (2021).

74. Kumar, M. & Gour, A. Novel approach to groundwater contaminant transport modelling. *J. Univ. Shanghai Sci. Technol.* **23**(7), 281–292 (2021).

75. Pareta, K., Reddy, T. & Singh, H. Geomorphological analysis of Ayad river basin, Udaipur (India) using remote sensing and GIS techniques. *Eur. J. Appl. Sci.* **10**(5), 423–442. https://doi.org/10.14738/aivp.105.12962 (2022).

76. Machiwal, D., Singh, P. K. & Yadav, K. K. Estimating aquifer properties and distributed groundwater recharge in a hard-rock catchment of Udaipur, India. *Appl. Water Sci.* **7**, 3157–3172. https://doi.org/10.1007/s13201-016-0462-8 (2016).

77. Wang, D., Wu, C., Huang, W. & Zhang, Y. Vibration investigation on fluid-structure interaction of AP1000 shield building subjected to multi earthquake excitations. *Ann. Nucl. Energy* **126**, 312–329. https://doi.org/10.1016/j.anucene.2018.11.021 (2019).

78. Baalousha, H. & Köngeter, J. Stochastic modelling and risk analysis of groundwater pollution using FORM coupled with automatic differentiation. *Adv. Water Resour.* **29**(12), 1815–1832. https://doi.org/10.1016/j.advwatres.2006.01.006 (2006).

79. Gedeon, G. *Groundwater Hydrology* (Continuing Education and Development (CED), Inc, 1999). https://www.cedengineering.com/userfiles/C09-002%20-%20Groundwater%20Hydrology%20-%20US.pdf

80. Reilly, T. E., & Harbaugh, A. W. *Guidelines for Evaluating Ground-Water Flow Models*. Scientific Investigations Report 2004-5038, Version 1.01 (U.S. Geological Survey, 2004). https://pubs.usgs.gov/sir/2004/5038/PDF/SIR20045038part2.pdf

81. Izady, A., Davary, K., Alizadeh, A. & Ziaei, A. A framework toward developing a groundwater conceptual model. *Arab. J. Geosci.* **7**(9), 3611–3631. https://doi.org/10.1007/s12517-013-0971-9 (2014).

82. Rusli, S. R. *et al.* Quantifying aquifer interaction using numerical groundwater flow model evaluated by environmental water tracer data: Application to the data-scarce area of the Bandung groundwater basin, West Java, Indonesia. *J. Hydrol. Region. Stud.* **50**, 1–26. https://doi.org/10.1016/j.ejrh.2023.101585 (2023).

83. Richards, L. A. Capillary conduction of liquids through porous mediums. *Physics* **1**(5), 318–333. https://doi.org/10.1063/1.1745010 (1931).

84. Anderson, M. P. & Woessner, W. W. *Applied Groundwater Modelling: Simulation of Flow and Advective Transport* (Academic Press, 1992).

85. Diersch, H. Finite-element modeling of recirculating density-driven saltwater intrusion processes in groundwater. *Adv. Water Resour.* **11**(1), 25–43 (1988).

86. Letniowski, F. W. & Forsyth, P. A. A control volume finite-element method for three-dimensional NAPL groundwater contamination. *Int. J. Numer. Methods Fluids* **13**(8), 955–970 (1991).

87. Raja Rao, C. S., Gupta, B. D., Iqbaluddin, P. B. C., Basu, K. K. & Dutta, A. K. Precambrian stratigraphy of Rajasthan—A review. *Rec. Geol. Survey India* **101**(2), 60–79 (1971).

88. Gupta, B. J. C. *Systematic Geological Mapping in Parts of Banswara and Chittorgarh Districts, Rajasthan* 1976–1977 (Geological Survey of India (GSI), FS, 1981).

89. Sahu, R. L. *Final Report on the Geology of Vindhyan Supergroup of South-Eastern Rajasthan* 1994 (Geological Survey of India (GSI), FS, 1995).

90. Heron, A. M. The geology of central Rajputana. *Mem. Geol. Surv. India* **79**, 1–389 (1953).

91. GSI. *Geological Map of Udaipur District at 1:50,000 Scale* (Geological Survey of India (GSI), 2001). https://bhukosh.gsi.gov.in/Bhukosh/MapViewer.aspx

92. CGWB. *Aquifer Mapping and Groundwater Management Plan Udaipur District, Rajasthan (Draft Report)* (Central Ground Water Board (CGWB), Ministry of Jal Shakti, Govt. of India, 2022). https://cgwb.gov.in/sites/default/files/2022-11/udaipur_final_compressed.pdf

93. WHO. *Guidelines for Drinking-Water Quality. 4th edition, Incorporating the 1st Addendum* (Public Health and the Environment, World Health Organization (WHO), 2017). https://www.who.int/publications/i/item/9789241549950

94. Freeze, R. A. & Cherry, J. A. *Groundwater* (Prentice Hall, 1979).

95. van Genuchten, MTh. A closed-form equation for predicting the hydraulic conductivity of unsaturated soils. *Soil Sci. Soc. Am. J.* **44**(5), 892–898. https://doi.org/10.2136/sssaj1980.03615995004400050002x (1980).

96. Leij, F. J., Alves, W. J., van Genuchten, M. Th., & Williams, J. R. *Unsaturated Soil Hydraulic Database, UNSODA 1.0 User's Manual*. Report EPA/600/R96/095 (US Environmental Protection Agency, 1996).

97. Doherty, J. Groundwater model calibration using pilot points and regularization. *Groundwater* **41**(2), 170–177. https://doi.org/10.1111/j.1745-6584.2003.tb02580.x (2003).

98. Doherty, J. *Calibration and Uncertainty Analysis for Complex Environmental Models* (Watermark Numerical Computing, 2015). Downloadable from www.pesthomepage.org.

99. Gelhar, L. W., Welty, C. & Rehfeldt, K. R. A critical review of data on field-scale dispersion in aquifers. *Water Resour. Res.* **28**(7), 1955–1974. https://doi.org/10.1029/92WR00607 (1992).

100. Helweg, O. J. & Labadie, J. W. Linked models for managing river basin salt balance. *Water Resour. Res.* **13**(2), 329–336 (1977).

101. Kies, B. *Solute Transport in Unsaturated Field Soil and in Groundwater*. Ph.D. dissertation, Department of Agronomy, New Mexico State University (1981).

102. Konikow, L. F. & Bredehoeft, J. D. Modelling flow and chemical quality changes in an irrigated stream-aquifer system. *Water Resour. Res.* **10**(3), 546–562 (1974).

103. Saltelli, A. *et al. Global Sensitivity Analysis* (Wiley, 2007). https://doi.org/10.1002/9780470725184.

104. ESH. *Three-Level, Mixed-Level and Fractional Factorial Designs, Engineering Statistics Handbook* (National Institute of Standards and Technology, US. Department of Commerce, 1991). https://www.itl.nist.gov/div898/handbook/pri/section3/pri33a.htm

Author contributions

The author confirms being the sole contributor of this work and has approved it for publication. I hereby provide consent for the publication of the manuscript detailed above, including any accompanying images or data contained within the manuscript that may directly or indirectly disclose my identity. I understand that this information will be freely available online, and accessible to the general public.

Competing interests

The author declares no competing interests.

Additional information

Correspondence and requests for materials should be addressed to K.P.

Reprints and permissions information is available at www.nature.com/reprints.

Publisher's note Springer Nature remains neutral with regard to jurisdictional claims in published maps and institutional affiliations.